Electrochemical push-pull probe: from scanning electrochemical microscopy (SECM) to multimodal altering of cell microenvironment.

SUPPORTING INFORMATION

Alexandra Bondarenko[1], Fernando Cortés-Salazar[1], Mihaela Gheorghiu[2], Szilveszter Gáspár[2], Dmitry Momotenko[1], Luciana Stanica[2,3], Andreas Lesch[1], Eugen Gheorghiu[2,3], Hubert H. Girault[1,*]

[1] Laboratoire d'Electrochimie Physique et Analytique, École Polytechnique Fédérale de Lausanne, Station 6, CH-1015 Lausanne, Switzerland.

[2]International Centre of Biodynamics, 1B IntrareaPortocalelor Street, 060101 Bucharest, Romania.

[3]Faculty of Biology, University of Bucharest, 91-95 Splaiul Independentei, Bucharest, Romania.

TABLE OF CONTENT

SI-I. Electrochemical characterization of the electrochemical push-pull probe.

Before carrying out experiments in the electrochemical mode, the ultramicroelectrode (UME) of the electrochemical push-pull probe was characterized by cyclic voltammetry (CV) in the presence of a solution of 2 mM FcMeOH in 0.1 M KNO_3 (Figures S1a). As it was expected, a sigmoidal electrochemical response indicating a clear steady-state current for the oxidation of FcMeOH was obtained with a relatively small capacitive current (Figure S1a). As it can be seen in Figure S1a, no significant difference was observed between the 1st and the 5th scan, which confirms the proper functioning of the carbon microelectrode and the possibility to generate electrochemically chemical effectors that might affect adherent cancer cells. Additionally, when the same experiment was carried out using Ag/AgCl/3 M KCl electrode the only effect observed was the shift of the potential towards more positive potentials by a value of 150 mV.

The optimal potential for water reduction was determined from CVs recorded with the electrochemical push-pull probe in 10 mM HEPES buffer solution, as the one shown in Figure S1b. The reduction of water was observed at potentials more negative than –1.8 V *vs* Ag-QRE as indicated by a drastic increase in the cathodic current. Besides the pH increasing, it was important to avoid H_2 bubble formation at the carbon UME. As a consequence, the working potential was selected only slightly more negative than –1.8 V (*i.e.* –2 V) *vs* Ag-QRE.

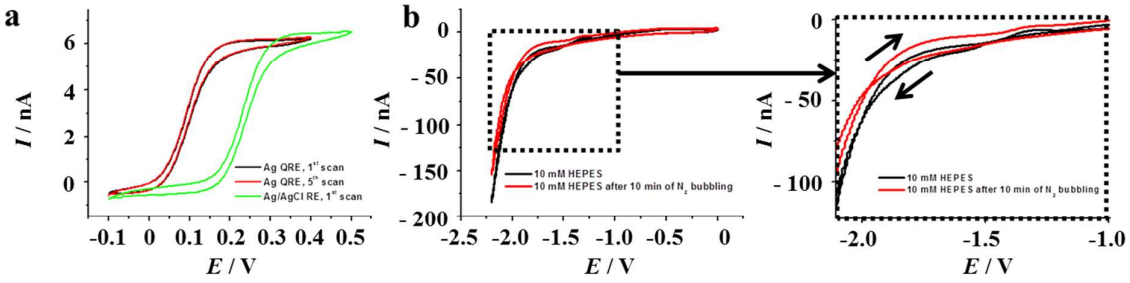

Figure S1 Cyclic voltammograms recorded with the electrochemical push-pull probe in 2 mM FcMeOH and 0.1 M KNO_3 (a) and 10 mM HEPES buffer (b). The inset represents a zoom-in on the highlighted area in Figure S1b. Working electrode = integrated carbon paste microelectrode, counter electrode (CE) = Pt, scan rate = 10 mV/s. As a reference electrode Ag wire (a and b) and Ag/AgCl/3 M KCl (a) standard electrode was used..

SI-II. Numerical simulations of the wall-jet electrode model

To corroborate the employed set of equations was solved appropriately, the well-known wall-jet electrode (WJE) system schematically presented in Figure S2a, was solved numerically and compared with the analytical solution. Herein, it is assumed that a compound A jetted perpendicularly to a planar disc electrode spreads radially over the surface (Figure S2b) and is converted into B as a result of an electrochemical reaction.

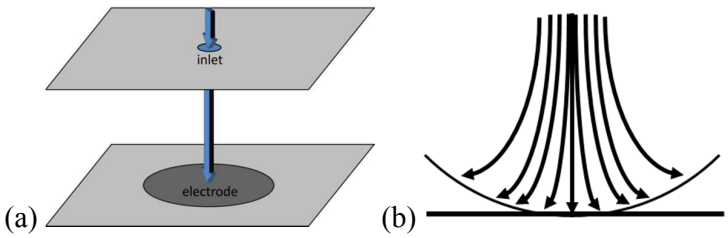

Figure S2. a) Wall-jet electrode scheme and b) flow velocity profiles around the electrode.

The analytical equation for the flow rate dependence of the transport-limited current for such system is:[1]

$$I = 1{,}59 k_c n F c_0 a^{-1/2} D^{2/3} \vartheta^{-5/12} V_f^{3/4} R^{3/4} \quad \text{(S1)}$$

where k_c is an experimental cell constant; n is the number of electrons in the redox reaction, F is the Faraday constant, c_0 is the bulk concentration of the electroactive species A, a is the diameter of the jet, D is the diffusion coefficient of the electroactive species, ϑ is the kinematic viscosity, V_f is the volume flow rate and R is the radius of the disc electrode. All WJE model parameters (Table S1) were chosen as described by Compton *et al.*[2]

Table S1. The values of the parameters used for the simulations and the analytical equation

Parameter	Value [units]	Name
ρ	1000 [kg/m^3]	water density
η	8.94×10^{-4} [Pa*s]	water viscosity
Flow rate	Variable from 1.7×10^{-4} to 1.7 [µL/min]	volume flow rate of compound A
A	$(\pi * a^2)/4$ [µm^2]	cross sectional surface area of the jet
linearFL	Flow rate/A	linear flow rate of compound A
D	1×10^{-9} [m^2/s]	diffusion coefficient
c_0	1 [mol/L]	initial concentration of compound A
k_c	1	experimental cell constant
n	1	the number of electrons in the redox reaction
F	96485 [C/mol]	Faraday constant
a	3.4×10^{-4} [m]	diameter of the jet
ϑ	1.004×10^{-6} [m^2/s]	kinematic viscosity

For the numerical simulations, the current at the disc electrode was calculated based on the total flux of the compound A that reaches the electrode surface. Therefore, three differential equations should be solved, as in the case of the electrochemical push pull probe, namely the convection-diffusion steady-state equations for both A and B compounds:

$$\nabla \cdot (-D\nabla c_A) = -\boldsymbol{u} \cdot \nabla c_A \tag{S2}$$

$$\nabla \cdot (-D\nabla c_B) = -\boldsymbol{u} \cdot \nabla c_B \tag{S3}$$

and the Navier-Stokes equation for compound A:

$$\rho(\boldsymbol{u} \cdot \nabla)\boldsymbol{u} = \nabla \cdot [-p\boldsymbol{I} + \eta(\nabla \boldsymbol{u} + (\nabla \boldsymbol{u})^T)] + \boldsymbol{F} \tag{S4}$$

where c_A and c_B are the concentrations of the compounds A and B at a given time, respectively, ρ is the density of the solution, η is the dynamic viscosity of the solution, $\boldsymbol{F}$ is a volume force, $\boldsymbol{u}$ is the flow velocity and $\boldsymbol{I}$ is the 3x3 identity matrix (see Table 1S for other parameters). Because the model has an axis of symmetry, the numerical simulations were simplified to a 2D symmetrical computational model. The boundary conditions employed are presented in Table S2.

Table S2. The boundary conditions for the differential equations employed to simulate the WJE system. Herein, $\boldsymbol{n}$ is the vector normal to the surface.

Surface	**Navier-Stokes**	**Convection-diffusion A**	**Convection-diffusion B**
Active surface of electrode	Wall, no slip; $\boldsymbol{u} = 0$	Flux; $-\boldsymbol{n} \cdot (-D\nabla c_A + c_A\boldsymbol{u}) = -k_1 * c_A$	Flux; $-\boldsymbol{n} \cdot (-D\nabla c_B + c_B\boldsymbol{u}) = -k_1 * c_A$
Jet	Inlet; Velocity; $\boldsymbol{u} = -U_0\boldsymbol{n}$; U_0 = linearFL	Concentration; $c_A = c_{A0}$; $c_{A0} = 1$ M	Concentration; $c_B = 0$
Box planes (with electrode and jet)	Wall, no slip; $\boldsymbol{u} = 0$	Insulation/Symmetry; $\boldsymbol{n} \cdot (-D\nabla c_A + c_A\boldsymbol{u}) = 0$	Insulation/Symmetry; $\boldsymbol{n} \cdot (-D\nabla c_A + c_A\boldsymbol{u}) = 0$
Box plane	Outlet, Pressure, no viscous stress, p = 0; $\eta(\nabla \boldsymbol{u} + (\nabla \boldsymbol{u})^T)\boldsymbol{n} = 0$	Convective flux; $\boldsymbol{n} \cdot (-D\nabla c_A) = 0$	Convective flux; $\boldsymbol{n} \cdot (-D\nabla c_B) = 0$

The numerical simulations were performed for a big range of volume flow rates: from 1.7 μL/min to 1.7×10^{-4} μL/min. The results from the numerical simulations presented a good

correlation with the ones obtained from the analytical equation and the experimental ones published by Compton *et al*.[2] For instance, the *I* values obtained at different flow rates for the numerical simulations (with an R^2 = 0.99975), presented a relative standard error on the slope relative to the data obtained through the analytical equation equal to 5% (Figure S3).

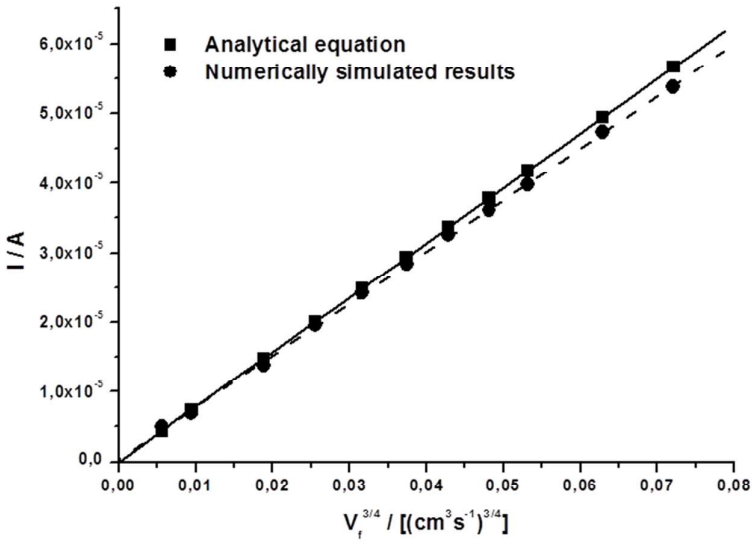

Figure S3. Comparison between the mass transport-limited currents calculated by using the analytical equation S1 and obtained *via* COMSOL numerical simulations.

SI-III. Numerical simulation of the electrochemical push-pull probe operated in the microfluidic mode.

To estimate theoretically the distribution over the sample surface of an active compound B that is delivered through the pushing channel and aspirated through the pulling channel of the electrochemical push-pull probe, the following two differential equations should be solved, namely the convection-diffusion (in steady-state) equation (S3) and the Navier-Stokes equation (S4), as described previously (SI-II). The values of the parameters used for the simulations are presented in Table S3.

Table S3. The values of the parameters used for the simulations of the microfluidic mode

Parameter	Value [units]	Name
ρ	1000 [kg/m^3]	water density
η	8.94×10^{-4} [Pa*s]	water viscosity
flowrate	1 [µL/min]	pushing volume flow rate
A	0.5*(70[µm]+100[µm])*30[µm]	cross sectional surface area of the microchannels
linearFL	Flow rate/A	pushing linear flow rate
linearFL2	linearFL [µL/min]*a (a = 1, 2, 3, 4, 5, 10)	aspirating linear flow rate
D	1×10^{-9} [m^2/s]	diffusion coefficient of compound B

The numerical solution of the system of differential equations was obtained by using the direct linear system solver UMFPACK with a relative error tolerance of 10^{-8} for the number of different distances between the probe and the substrate pattern. To reduce the RAM amount required for simulations and allow the numerical solution to converge, which is particularly difficult with coupled Navier-Stokes and diffusion-convection equations, the "stored solution options" were used. The boundary conditions listed in Table S4 were employed.

Table S4. The boundary conditions for the differential equations employed for the simulations of the microfluidic mode of the electrochemical push-pull probe. Herein, $\boldsymbol{n}$ is the vector normal to the surface.

Surface	**Navier-Stokes**	**Convection-diffusion B**
Active surface of electrode	Wall; no slip; $\boldsymbol{u} = 0$	Insulation/Symmetry; $\boldsymbol{n} \cdot (-D\nabla c_B + c_B\boldsymbol{u}) = 0$
Body of the probe	Wall; no slip; $\boldsymbol{u} = 0$	Insulation/Symmetry; $\boldsymbol{n} \cdot (-D\nabla c_B + c_B\boldsymbol{u}) = 0$
Box planes (except reactive pattern)	Wall; no slip; $\boldsymbol{u} = 0$	Concentration; $c_B = 0$
Substrate pattern	Wall; no slip; $\boldsymbol{u} = 0$	Insulation/Symmetry; $\boldsymbol{n} \cdot (-D\nabla c_B + c_B\boldsymbol{u}) = 0$
Pushing microchannel	Inlet; Velocity; $\boldsymbol{u} = -U_0\boldsymbol{n}$;	Concentration; $c_B = c_{B0}$; $c_{B0} = 1$ M

	U_0 = linearFL	
Aspirating microchannel	Outlet; Velocity; $\boldsymbol{u} = -U_0\boldsymbol{n}$; U_0 = linearFL×X, X=1, 2, 3, 4, 5, 10	Convective flux; $\boldsymbol{n} \cdot (-D\nabla c_B) = 0$

The results of the numerical simulations are presented in Figure S4 and Figure S5, as well as, in the main manuscript Figure 2. The numerical simulations demonstrated a significant influence of the inclination angle, the working distance and the aspiration rate on the affected area of the sample. For more details see Results and discussion, Computational model and numerical simulations.

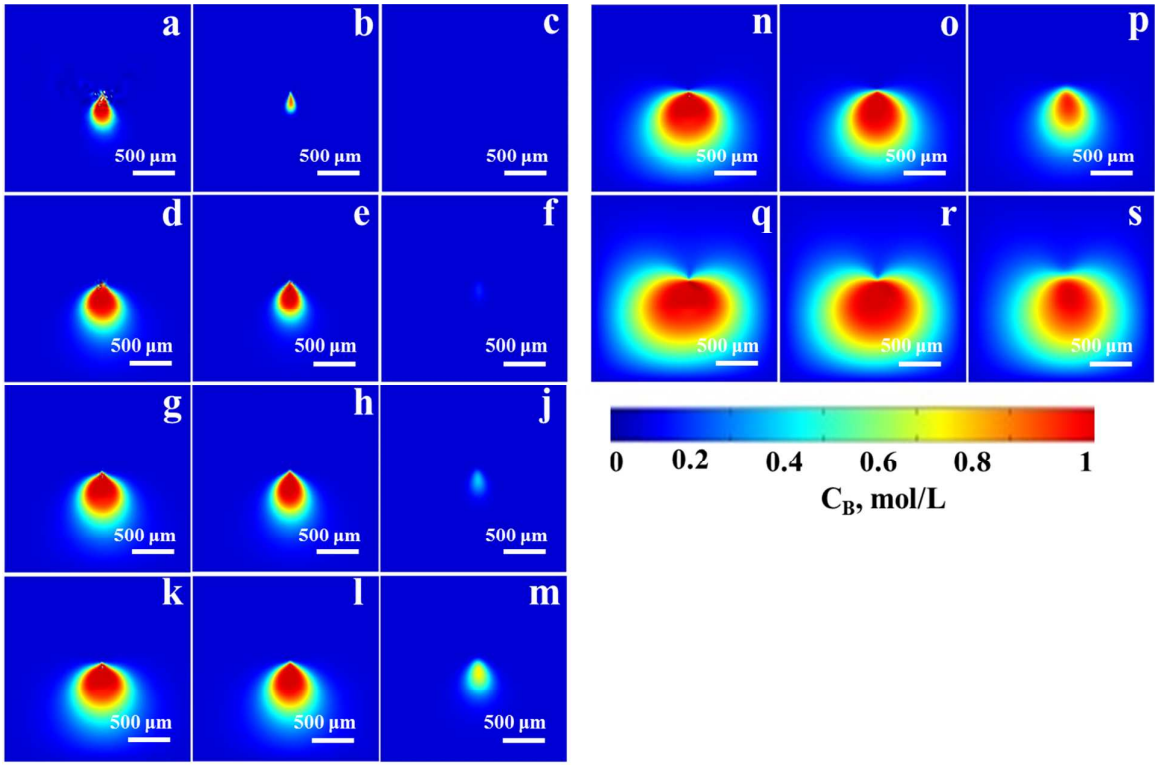

Figure S4. Simulated concentration profiles of the active compound B delivered over the sample surface by the electrochemical push-pull probe operated under different conditions. The pushing flow rate was 1 µL/min for all the simulations and the inclination angle 90°. The aspirating flow rate and the working distance *d* for each case were: a) 10 µL/min, 50 µm; b) 10 µL/min, 100 µm; c) 10 µL/min, 250 µm; d) 5 µL/min, 50 µm; e) 5 µL/min, 100 µm; f) 5 µL/min, 250 µm; g) 4 µL/min, 50 µm; h) 4 µL/min, 100 µm; j) 4 µL/min, 250 µm; k) 3 µL/min, 50 µm; l) 3 µL/min, 100 µm; m) 3 µL/min, 250 µm; n) 2 µL/min, 50 µm; o) 2 µL/min, 100 µm; p) 2 µL/min, 250 µm; q) 1 µL/min, 50 µm; r) 1 µL/min, 100 µm; s) 1 µL/min, 250 µm.

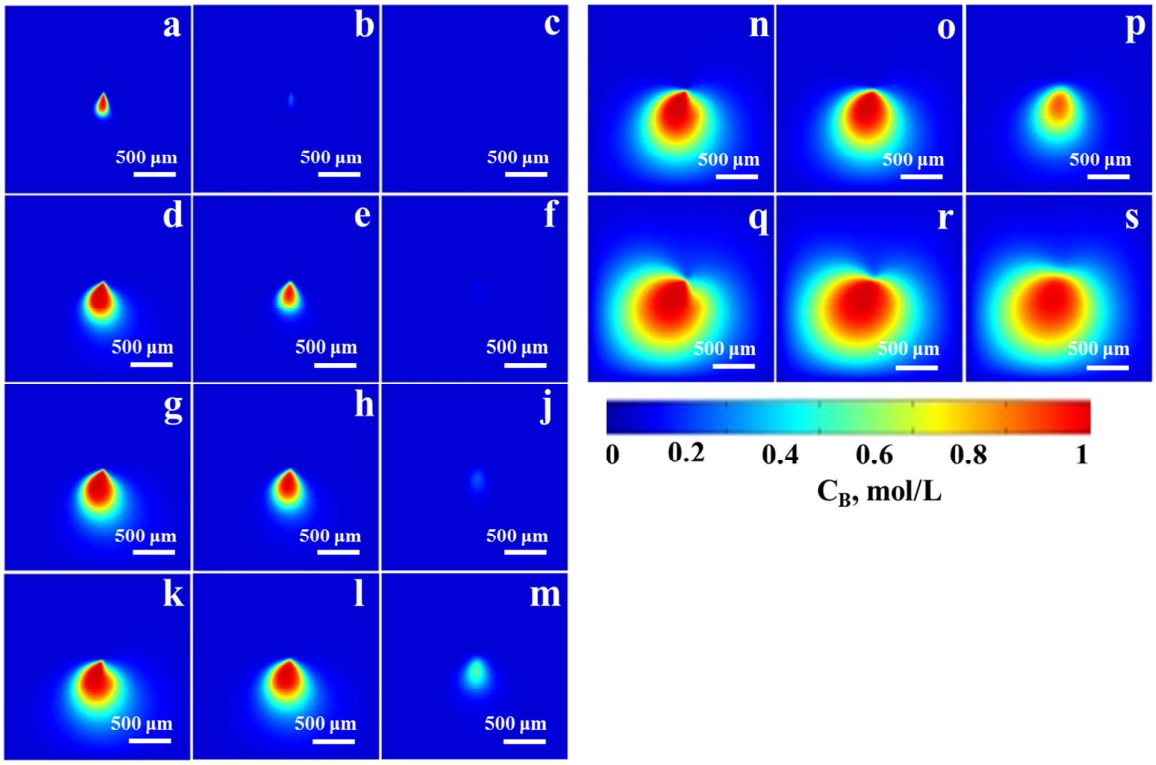

Figure S5. Simulated concentration profiles of the active compound B delivered over the sample surface by the electrochemical push-pull probe operated under different conditions. The pushing flow rate was 1 µL/min for all the simulations and the inclination angle 70°. The aspirating flow rate and the working distance *d* for each case were: a) 10 µL/min, 50 µm; b) 10 µL/min, 100 µm; c) 10 µL/min, 250 µm; d) 5 µL/min, 50 µm; e) 5 µL/min, 100 µm; f) 5 µL/min, 250 µm; g) 4 µL/min, 50 µm; h) 4 µL/min, 100 µm; j) 4 µL/min, 250 µm; k) 3 µL/min, 50 µm; l) 3 µL/min, 100 µm; m) 3 µL/min, 250 µm; n) 2 µL/min, 50 µm; o) 2 µL/min, 100 µm; p) 2 µL/min, 250 µm; q) 1 µL/min, 50 µm; r) 1 µL/min, 100 µm; s) 1 µL/min, 250 µm.

Typical COMSOL Model Report for the simulations of Navier-Stokes equation. The working distance *d* was equal to 100 µm, the inclination angle was equal to 90°, the pushing and aspirating flow rates were 1 µL/min and 10 µL/min respectively.

COMSOL Model Report

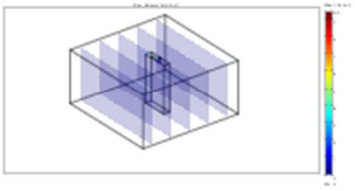

1. Table of Contents

2. Model Properties

Property	**Value**
Model name	
Author	
Company	

Department	
Reference	
URL	
Saved date	Mar 17, 2015 4:54:56 PM
Creation date	Nov 20, 2012 10:02:44 AM
COMSOL version	COMSOL 3.5.0.603

File name: /home/dmitry/Desktop/Alexandra/Corrections/N-S_example.mph

Application modes and modules used in this model:

- Geom1 (3D)
    - Convection and Diffusion
    - Incompressible Navier-Stokes (Chemical Engineering Module)

3. Constants

Name	**Expression**	**Value**	**Description**
rho	1000[kg/m^3]	1000[kg/m^3]	density of water
nu	8.94e-4[Pa*s]	(8.94e-4)[kg/(m·s)]	water viscosity
flowrate	1[uL/min]	(1.666667e-11)[m^3/s]	volumic flowrate
A	0.5*170[um]*30[um]	(2.55e-9)[m^2]	cross sectional surface area of capilary
linearFL	flowrate/A	0.006536[m/s]	linear flowrate
Diff	1e-9[m^2/s]	(1e-9)[m^2/s]	diffusion coefficient for analyte
c0	1[mol/L]	1000[mol/m^3]	initial analyte concentration
f	1	1	flowrate factor

linearFL2	linearFL*10	0.065359[m/s]	pulling

4. Geometry

Number of geometries: 1

4.1. Geom1

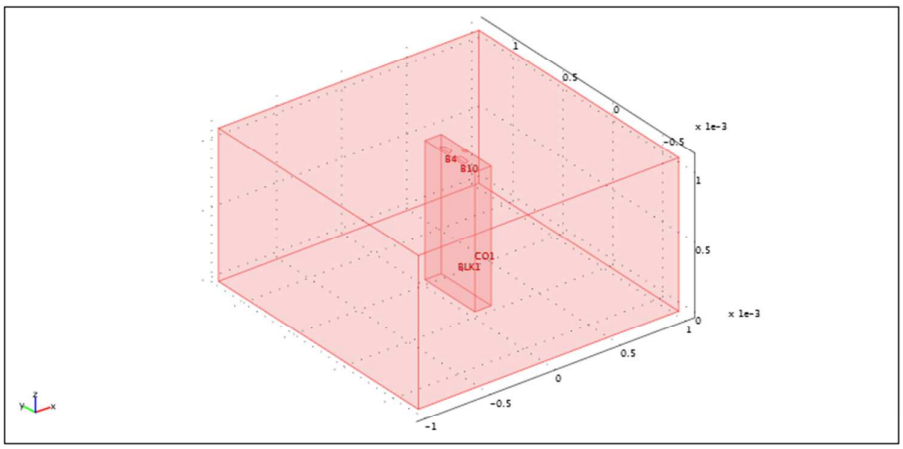

4.1.1. Point mode

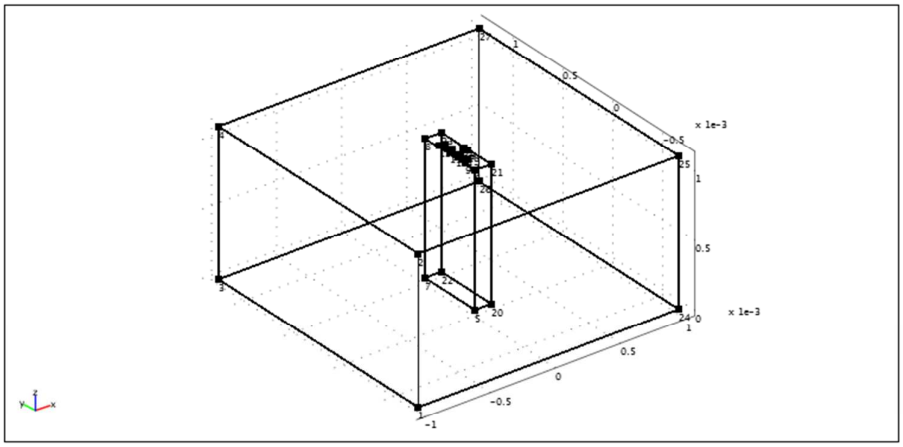

4.1.2. Edge mode

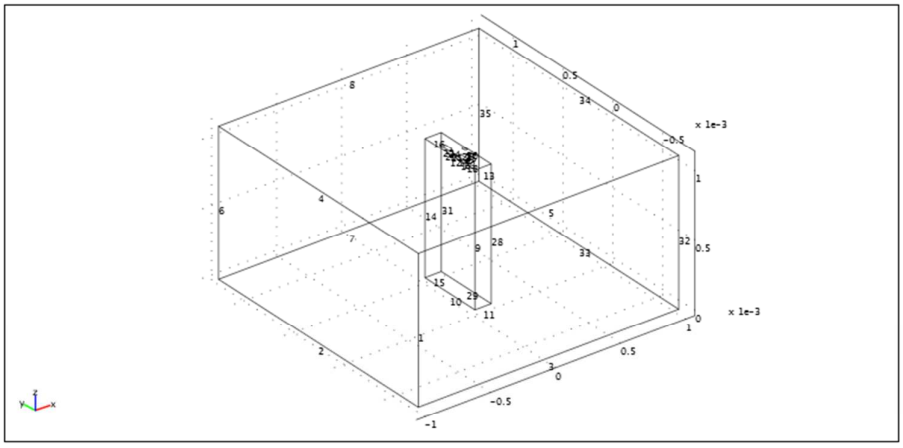

4.1.3. Boundary mode

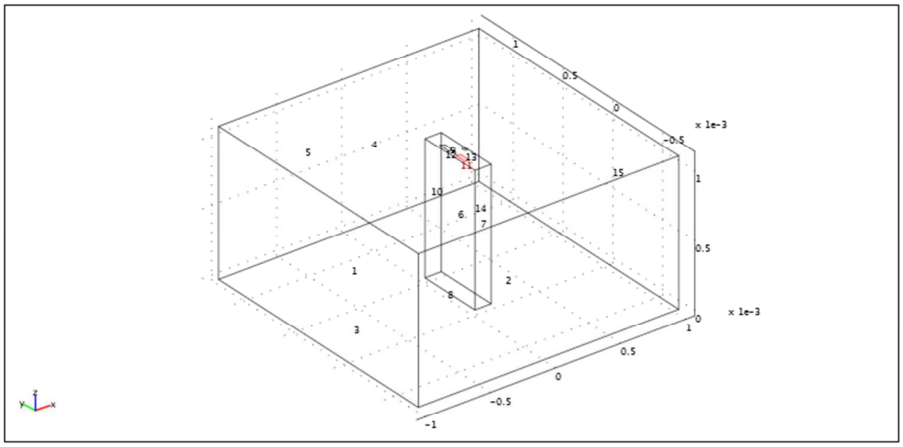

4.1.4. Subdomain mode

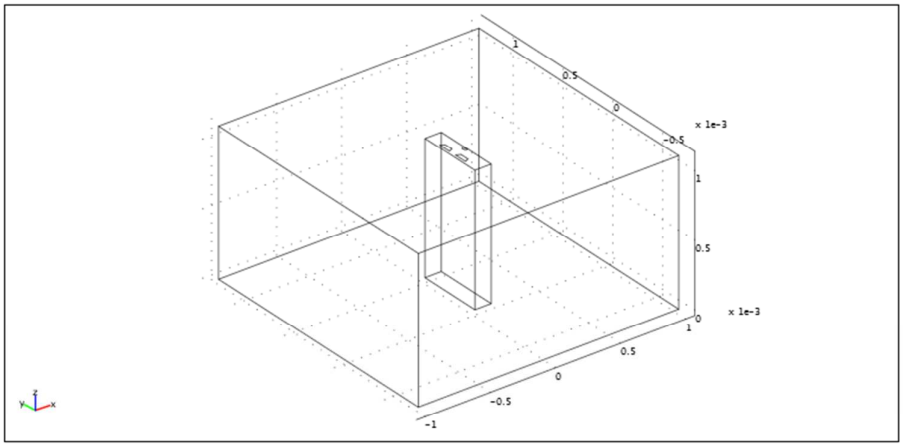

5. Geom1

Space dimensions: 3D

Independent variables: x, y, z

5.1. Mesh

5.1.1. Mesh Statistics

Number of degrees of freedom	168890
Number of mesh points	6286
Number of elements	26710
Tetrahedral	26710
Prism	0
Hexahedral	0
Number of boundary elements	7586
Triangular	7586
Quadrilateral	0
Number of edge elements	318
Number of vertex elements	27
Minimum element quality	0.246
Element volume ratio	0

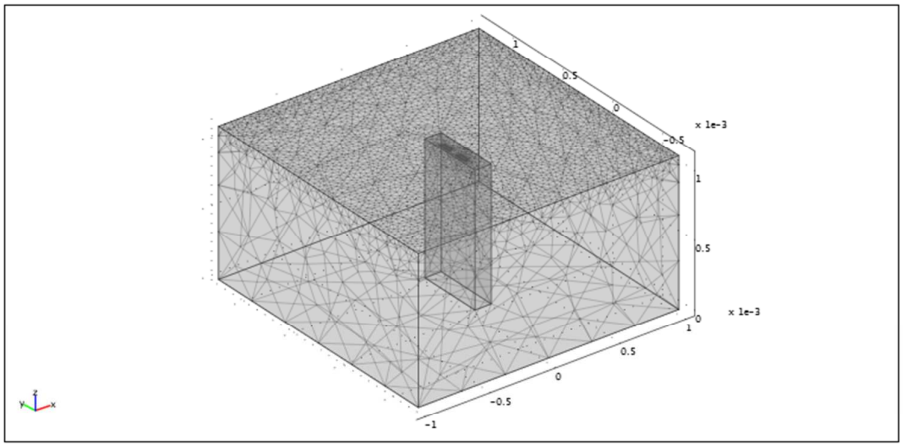

5.2. Application Mode: Convection and Diffusion (cd)

Application mode type: Convection and Diffusion

Application mode name: cd

5.2.1. Application Mode Properties

Property	**Value**
Default element type	Lagrange - Quadratic
Analysis type	Stationary
Equation form	Non-conservative
Frame	Frame (ref)
Weak constraints	Off
Constraint type	Ideal

5.2.2. Variables

Dependent variables: c

Shape functions: shlag(2,'c')

Interior boundaries not active

5.2.3. Boundary Settings

Boundary		1-3, 5, 15	4, 6-7, 9-10, 14	11
Type		Concentration	Insulation/Symmetry	Concentration
Concentration (c0)	mol/m^3	0	0	**c0**

Boundary		12	13
Type		Convective flux	Insulation/Symmetry
Concentration (c0)	mol/m^3	0	**c0**

5.2.4. Subdomain Settings

Subdomain		1
Diffusion coefficient (D)	m^2/s	**Diff**
x-velocity (u)	m/s	**u**
y-velocity (v)	m/s	**v**
z-velocity (w)	m/s	**w**

5.3. Application Mode: Incompressible Navier-Stokes (chns)

Application mode type: Incompressible Navier-Stokes (Chemical Engineering Module)

Application mode name: chns

5.3.1. Scalar Variables

Name	Variable	Value	Unit	Description
visc_vel_fact	visc_vel_fact_chns	10	1	Viscous velocity factor

5.3.2. Application Mode Properties

Property	**Value**
Default element type	Lagrange - P_2 P_1
Analysis type	Stationary
Corner smoothing	Off
Weakly compressible flow	Off
Turbulence model	None
Realizability	Off
Non-Newtonian flow	Off
Brinkman on by default	Off
Two-phase flow	Single-phase flow
Frame	Frame (ref)
Weak constraints	Off
Constraint type	Ideal

5.3.3. Variables

Dependent variables: u, v, w, p, logk, logd, logw, phi, psi, nxw, nyw, nzw

Shape functions: shlag(2,'u'), shlag(2,'v'), shlag(2,'w'), shlag(1,'p')

Interior boundaries not active

5.3.4. Boundary Settings

Boundary		1-3, 5, 15	4, 6-7, 9-10, 13-14	11
Type		Outlet	Wall	Inlet
outtype		Pressure, no viscous stress	Pressure, no viscous stress	Pressure, no viscous stress
Normal inflow velocity (U0in)	m/s	1	1	**linearFL**
Normal outflow velocity (U0out)	m/s	0	0	0

Boundary		12
Type		Outlet
outtype		**Velocity**
Normal inflow velocity (U0in)	m/s	1
Normal outflow velocity (U0out)	m/s	**linearFL2**

5.3.5. Subdomain Settings

Subdomain		1
Integration order (gporder)		**4 4 4 2**
Constraint order (cporder)		**2 2 2 1**
Density (rho)	kg/m^3	**rho**
Dynamic viscosity (eta)	Pa·s	**nu**

6. Solver Settings

Solve using a script: off

Analysis type	Stationary
Auto select solver	On
Solver	Stationary
Solution form	Automatic
Symmetric	Off
Adaptive mesh refinement	Off
Optimization/Sensitivity	Off
Plot while solving	Off

6.1. Direct (UMFPACK)

Solver type: Linear system solver

Parameter	**Value**
Pivot threshold	0.1
Memory allocation factor	0.7

6.2. Stationary

Parameter	**Value**
Linearity	Automatic
Relative tolerance	1.0E-8
Maximum number of iterations	50

Manual tuning of damping parameters	On
Highly nonlinear problem	On
Initial damping factor	1.0E-4
Minimum damping factor	1.0E-12
Restriction for step size update	10.0

6.3. Advanced

Parameter	**Value**
Constraint handling method	Elimination
Null-space function	Automatic
Automatic assembly block size	On
Assembly block size	1000
Use Hermitian transpose of constraint matrix and in symmetry detection	Off
Use complex functions with real input	Off
Stop if error due to undefined operation	On
Store solution on file	Off
Type of scaling	Automatic
Manual scaling	
Row equilibration	On
Manual control of reassembly	Off
Load constant	On
Constraint constant	On

Mass constant	On
Damping (mass) constant	On
Jacobian constant	On
Constraint Jacobian constant	On

7. Postprocessing

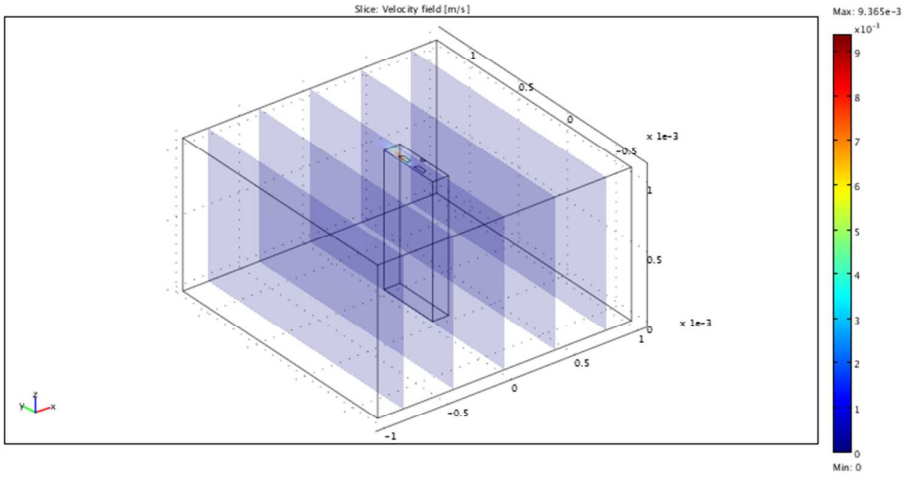

8. Variables

8.1. Boundary

8.1.1. Boundary 1-7, 9-15

Name	Description	Unit	Expression
ndflux_c_cd	Normal diffusive flux, c	mol/(m^2*s)	nx_cd * dflux_c_x_cd+ny_cd * dflux_c_y_cd+nz_cd * dflux_c_z_cd
ncflux_c_cd	Normal convective flux, c	mol/(m^2*s)	nx_cd * cflux_c_x_cd+ny_cd * cflux_c_y_cd+nz_cd * cflux_c_z_cd

ntflux_c_cd	Normal total flux, c	mol/(m^2*s)	nx_cd * tflux_c_x_cd+ny_cd * tflux_c_y_cd+nz_cd * tflux_c_z_cd
K_x_chns	Viscous force per area, x component	Pa	eta_chns * (2 * nx_chns * ux+ny_chns * (uy+vx)+nz_chns * (uz+wx))
T_x_chns	Total force per area, x component	Pa	-nx_chns * p+2 * nx_chns * eta_chns * ux+ny_chns * eta_chns * (uy+vx)+nz_chns * eta_chns * (uz+wx)
K_y_chns	Viscous force per area, y component	Pa	eta_chns * (nx_chns * (vx+uy)+2 * ny_chns * vy+nz_chns * (vz+wy))
T_y_chns	Total force per area, y component	Pa	-ny_chns * p+nx_chns * eta_chns * (vx+uy)+2 * ny_chns * eta_chns * vy+nz_chns * eta_chns * (vz+wy)
K_z_chns	Viscous force per area, z component	Pa	eta_chns * (nx_chns * (wx+uz)+ny_chns * (wy+vz)+2 * nz_chns * wz)
T_z_chns	Total force per area, z component	Pa	-nz_chns * p+nx_chns * eta_chns * (wx+uz)+ny_chns * eta_chns * (wy+vz)+2 * nz_chns * eta_chns * wz

8.1.2. Boundary 8

Name	**Description**	**Unit**	**Expression**
ndflux_c_cd	Normal diffusive flux, c	mol/(m^2*s)	
ncflux_c_cd	Normal convective flux, c	mol/(m^2*s)	
ntflux_c_cd	Normal total flux, c	mol/(m^2*s)	
K_x_chns	Viscous force per area, x component	Pa	

T_x_chns	Total force per area, x component	Pa	
K_y_chns	Viscous force per area, y component	Pa	
T_y_chns	Total force per area, y component	Pa	
K_z_chns	Viscous force per area, z component	Pa	
T_z_chns	Total force per area, z component	Pa	

8.2. Subdomain

8.2.1. Subdomain 1

Name	**Description**	**Unit**	**Expression**
grad_c_x_cd	Concentration gradient, c, x component	mol/m^4	cx
dflux_c_x_cd	Diffusive flux, c, x component	mol/(m^2*s)	-Dxx_c_cd * cx-Dxy_c_cd * cy-Dxz_c_cd * cz
cflux_c_x_cd	Convective flux, c, x component	mol/(m^2*s)	c * u_c_cd
tflux_c_x_cd	Total flux, c, x component	mol/(m^2*s)	dflux_c_x_cd+cflux_c_x_cd
grad_c_y_cd	Concentration gradient,	mol/m^4	cy

	c, y component		
dflux_c_y_cd	Diffusive flux, c, y component	mol/(m^2*s)	-Dyx_c_cd * cx-Dyy_c_cd * cy-Dyz_c_cd * cz
cflux_c_y_cd	Convective flux, c, y component	mol/(m^2*s)	c * v_c_cd
tflux_c_y_cd	Total flux, c, y component	mol/(m^2*s)	dflux_c_y_cd+cflux_c_y_cd
grad_c_z_cd	Concentration gradient, c, z component	mol/m^4	cz
dflux_c_z_cd	Diffusive flux, c, z component	mol/(m^2*s)	-Dzx_c_cd * cx-Dzy_c_cd * cy-Dzz_c_cd * cz
cflux_c_z_cd	Convective flux, c, z component	mol/(m^2*s)	c * w_c_cd
tflux_c_z_cd	Total flux, c, z component	mol/(m^2*s)	dflux_c_z_cd+cflux_c_z_cd

beta_c_x_cd	Convective field, c, x component	m/s	u_c_cd
beta_c_y_cd	Convective field, c, y component	m/s	v_c_cd
beta_c_z_cd	Convective field, c, z component	m/s	w_c_cd
grad_c_cd	Concentration gradient, c	mol/m^4	sqrt(grad_c_x_cd^2+grad_c_y_cd^2+grad_c_z_cd^2)
dflux_c_cd	Diffusive flux, c	mol/(m^2*s)	sqrt(dflux_c_x_cd^2+dflux_c_y_cd^2+dflux_c_z_cd^2)
cflux_c_cd	Convective flux, c	mol/(m^2*s)	sqrt(cflux_c_x_cd^2+cflux_c_y_cd^2+cflux_c_z_cd^2)
tflux_c_cd	Total flux, c	mol/(m^2*s)	sqrt(tflux_c_x_cd^2+tflux_c_y_cd^2+tflux_c_z_cd^2)
cellPe_c_cd	Cell Peclet number, c	1	h * sqrt(beta_c_x_cd^2+beta_c_y_cd^2+beta_c_z_cd^2)/Dm_c_cd
Dm_c_cd	Mean diffusion coefficient,	m^2/s	(Dxx_c_cd * u_c_cd^2+Dxy_c_cd * u_c_cd * v_c_cd+Dxz_c_cd * u_c_cd * w_c_cd+Dyx_c_cd * v_c_cd * u_c_cd+Dyy_c_cd * v_c_cd^2+Dyz_c_cd *

	c		v_c_cd * w_c_cd+Dzx_c_cd * w_c_cd * u_c_cd+Dzy_c_cd * w_c_cd * v_c_cd+Dzz_c_cd * w_c_cd^2)/(u_c_cd^2+v_c_cd^2+w_c_cd^2+eps)
res_c_cd	Equation residual for c	mol/(m^3*s)	-Dxx_c_cd * cxx-Dxy_c_cd * cxy-Dxz_c_cd * cxz+cx * u_c_cd-Dyx_c_cd * cyx-Dyy_c_cd * cyy-Dyz_c_cd * cyz+cy * v_c_cd-Dzx_c_cd * czx-Dzy_c_cd * czy-Dzz_c_cd * czz+cz * w_c_cd-R_c_cd
res_sc_c_cd	Shock capturing residual for c	mol/(m^3*s)	cx * u_c_cd+cy * v_c_cd+cz * w_c_cd-R_c_cd
da_c_cd	Total time scale factor, c	1	Dts_c_cd
U_chns	Velocity field	m/s	sqrt(u^2+v^2+w^2)
Vx_chns	Vorticity, x component	1/s	wy-vz
Vy_chns	Vorticity, y component	1/s	uz-wx
Vz_chns	Vorticity, z component	1/s	vx-uy
V_chns	Vorticity	1/s	sqrt(Vx_chns^2+Vy_chns^2+Vz_chns^2)
divU_chns	Divergence	1/s	ux+vy+wz

	of velocity field		
cellRe_chns	Cell Reynolds number	1	rho_chns * U_chns * h/eta_chns
res_u_chns	Equation residual for u	N/m^3	rho_chns * (u * ux+v * uy+w * uz)+px-F_x_chns+if(gmg_level>0,0,-eta_chns * (2 * uxx+uyy+vxy+uzz+wxz))
res_v_chns	Equation residual for v	N/m^3	rho_chns * (u * vx+v * vy+w * vz)+py-F_y_chns+if(gmg_level>0,0,-eta_chns * (vxx+uyx+2 * vyy+vzz+wyz))
res_w_chns	Equation residual for w	N/m^3	rho_chns * (u * wx+v * wy+w * wz)+pz-F_z_chns+if(gmg_level>0,0,-eta_chns * (wxx+uzx+wyy+vzy+2 * wzz))
beta_x_chns	Convective field, x component	kg/(m^2*s)	rho_chns * u
beta_y_chns	Convective field, y component	kg/(m^2*s)	rho_chns * v
beta_z_chns	Convective field, z component	kg/(m^2*s)	rho_chns * w
Dm_chns	Mean	Pa*s	eta_chns

	diffusion coefficient		
da_chns	Total time scale factor	kg/m^3	rho_chns
taum_chns	GLS time-scale	m^3*s/kg	nojac(1/max(2 * rho_chns * sqrt(emetric(u,v,w)),48 * eta_chns/h^2))
tauc_chns	GLS time-scale	m^2/s	0.5 * nojac(if(u^2+v^2+w^2<="" td="">
res_p_chns	Equation residual for p	kg/(m^3*s)	rho_chns * divU_chns

8.2.2. Subdomain 2

Name	**Description**	**Unit**	**Expression**
grad_c_x_cd	Concentration gradient, c, x component	mol/m^4	
dflux_c_x_cd	Diffusive flux, c, x component	mol/(m^2*s)	
cflux_c_x_cd	Convective flux, c, x component	mol/(m^2*s)	
tflux_c_x_cd	Total flux, c, x component	mol/(m^2*s)	
grad_c_y_cd	Concentration gradient, c, y component	mol/m^4	
dflux_c_y_cd	Diffusive flux, c, y component	mol/(m^2*s)	
cflux_c_y_cd	Convective flux, c, y component	mol/(m^2*s)	
tflux_c_y_cd	Total flux, c, y component	mol/(m^2*s)	
grad_c_z_cd	Concentration gradient, c, z component	mol/m^4	

dflux_c_z_cd	Diffusive flux, c, z component	mol/(m^2*s)	
cflux_c_z_cd	Convective flux, c, z component	mol/(m^2*s)	
tflux_c_z_cd	Total flux, c, z component	mol/(m^2*s)	
beta_c_x_cd	Convective field, c, x component	m/s	
beta_c_y_cd	Convective field, c, y component	m/s	
beta_c_z_cd	Convective field, c, z component	m/s	
grad_c_cd	Concentration gradient, c	mol/m^4	
dflux_c_cd	Diffusive flux, c	mol/(m^2*s)	
cflux_c_cd	Convective flux, c	mol/(m^2*s)	
tflux_c_cd	Total flux, c	mol/(m^2*s)	
cellPe_c_cd	Cell Peclet number, c	1	
Dm_c_cd	Mean diffusion coefficient, c	m^2/s	
res_c_cd	Equation residual for c	mol/(m^3*s)	
res_sc_c_cd	Shock capturing residual for c	mol/(m^3*s)	
da_c_cd	Total time scale factor, c	1	
U_chns	Velocity field	m/s	
Vx_chns	Vorticity, x component	1/s	
Vy_chns	Vorticity, y component	1/s	
Vz_chns	Vorticity, z component	1/s	
V_chns	Vorticity	1/s	
divU_chns	Divergence of velocity field	1/s	
cellRe_chns	Cell Reynolds number	1	

res_u_chns	Equation residual for u	N/m^3	
res_v_chns	Equation residual for v	N/m^3	
res_w_chns	Equation residual for w	N/m^3	
beta_x_chns	Convective field, x component	kg/(m^2*s)	
beta_y_chns	Convective field, y component	kg/(m^2*s)	
beta_z_chns	Convective field, z component	kg/(m^2*s)	
Dm_chns	Mean diffusion coefficient	Pa*s	
da_chns	Total time scale factor	kg/m^3	
taum_chns	GLS time-scale	m^3*s/kg	
tauc_chns	GLS time-scale	m^2/s	
res_p_chns	Equation residual for p	kg/(m^3*s)	

Typical COMSOL Model Report for the simulations of convection-diffusion equation. The working distance *d* was equal to 100 µm, the inclination angle was equal to 90°, the pushing and aspirating flow rates were 1 µL/min and 10 µL/min respectively.

COMSOL Model Report

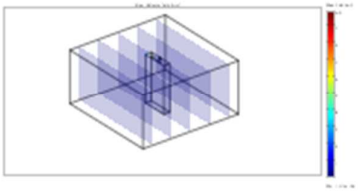

1. Table of Contents

2. Model Properties

Property	**Value**
Model name	
Author	
Company	

Department	
Reference	
URL	
Saved date	Mar 17, 2015 5:00:47 PM
Creation date	Nov 20, 2012 10:02:44 AM
COMSOL version	COMSOL 3.5.0.603

File name: /home/dmitry/Desktop/Alexandra/Corrections/C-D_example.mph

Application modes and modules used in this model:

- Geom1 (3D)
    - Convection and Diffusion
    - Incompressible Navier-Stokes (Chemical Engineering Module)

3. Constants

Name	**Expression**	**Value**	**Description**
rho	1000[kg/m^3]	1000[kg/m^3]	density of water
nu	8.94e-4[Pa*s]	(8.94e-4)[kg/(m·s)]	water viscosity
flowrate	1[uL/min]	(1.666667e-11)[m^3/s]	volumic flowrate
A	0.5*170[um]*30[um]	(2.55e-9)[m^2]	cross sectional surface area of capilary
linearFL	flowrate/A	0.006536[m/s]	linear flowrate
Diff	1e-9[m^2/s]	(1e-9)[m^2/s]	diffusion coefficient for analyte
c0	1[mol/L]	1000[mol/m^3]	initial analyte concentration
f	1	1	flowrate factor

linearFL2	linearFL*10	0.065359[m/s]	pulling

4. Geometry

Number of geometries: 1

4.1. Geom1

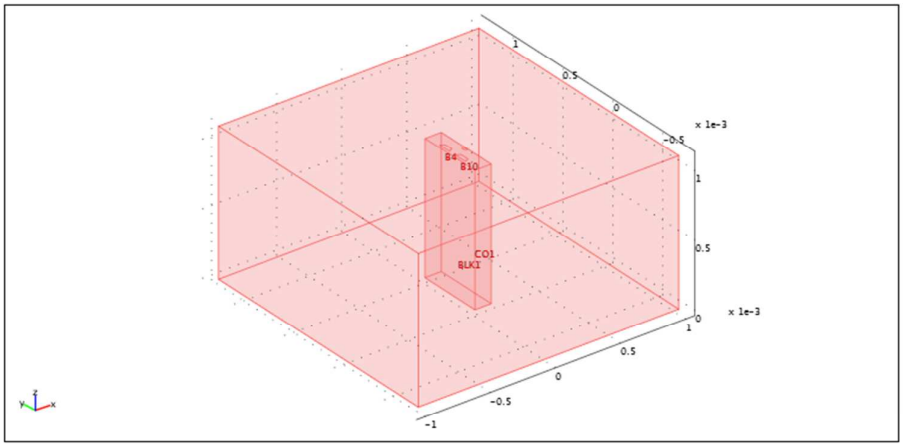

4.1.1. Point mode

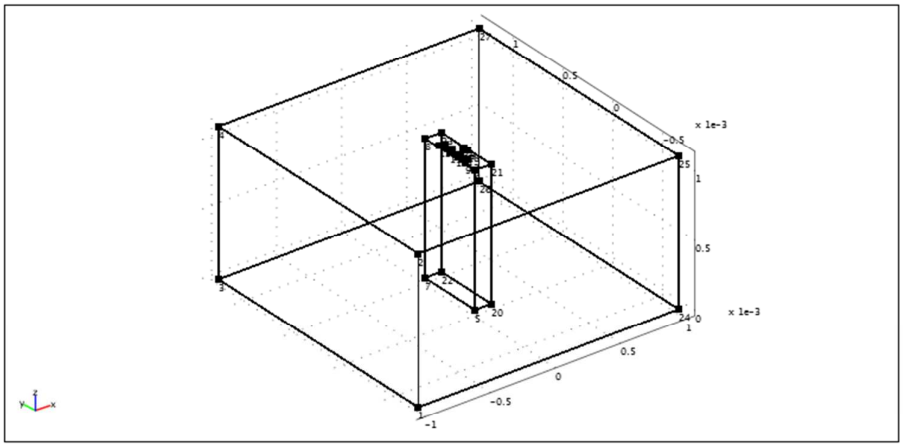

4.1.2. Edge mode

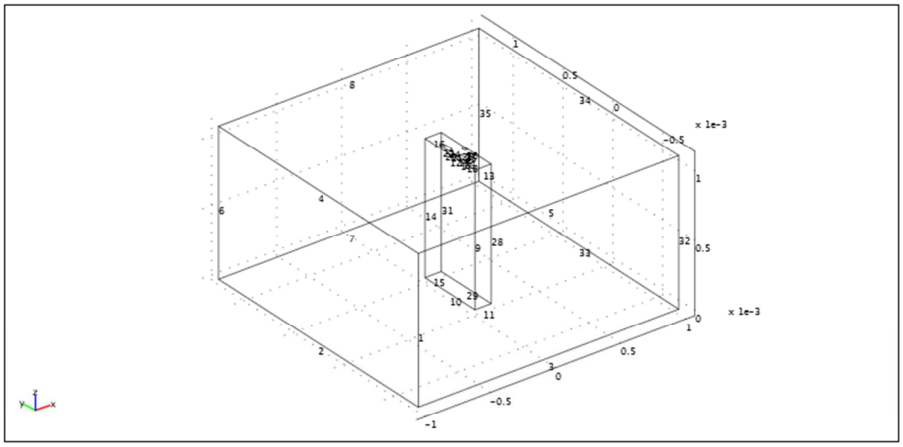

4.1.3. Boundary mode

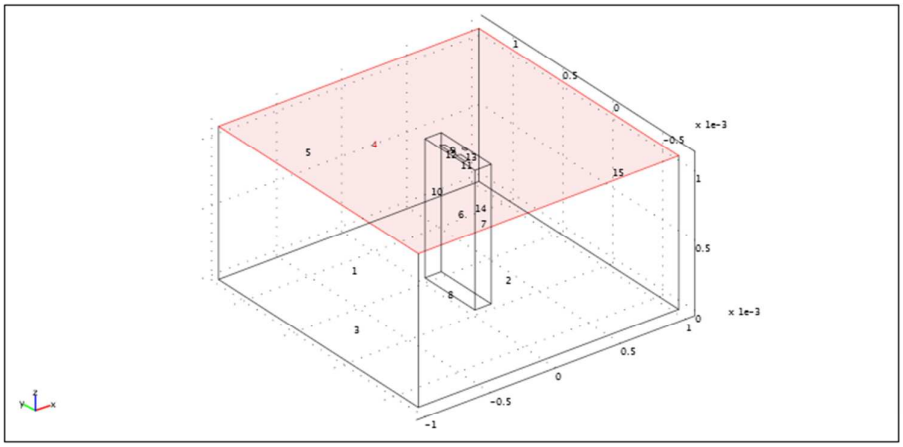

4.1.4. Subdomain mode

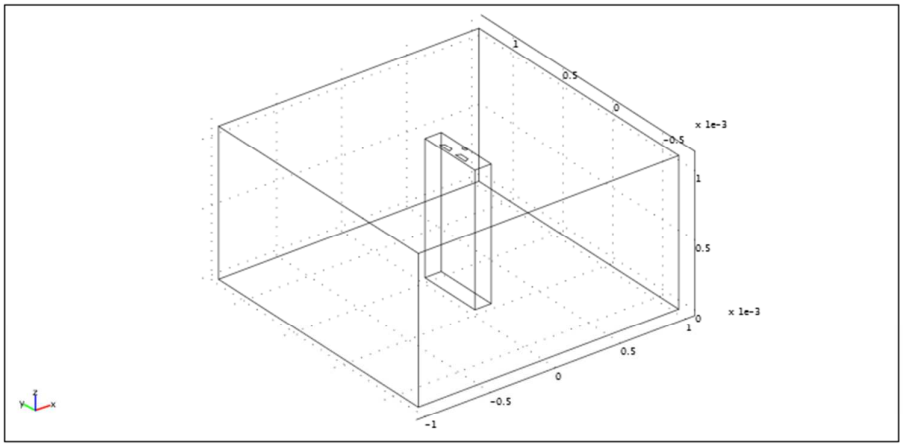

5. Geom1

Space dimensions: 3D

Independent variables: x, y, z

5.1. Mesh

5.1.1. Mesh Statistics

Number of degrees of freedom	1822912
Number of mesh points	65421
Number of elements	272162
Tetrahedral	272162
Prism	0
Hexahedral	0
Number of boundary elements	77696
Triangular	77696
Quadrilateral	0
Number of edge elements	740
Number of vertex elements	27
Minimum element quality	0.25
Element volume ratio	0

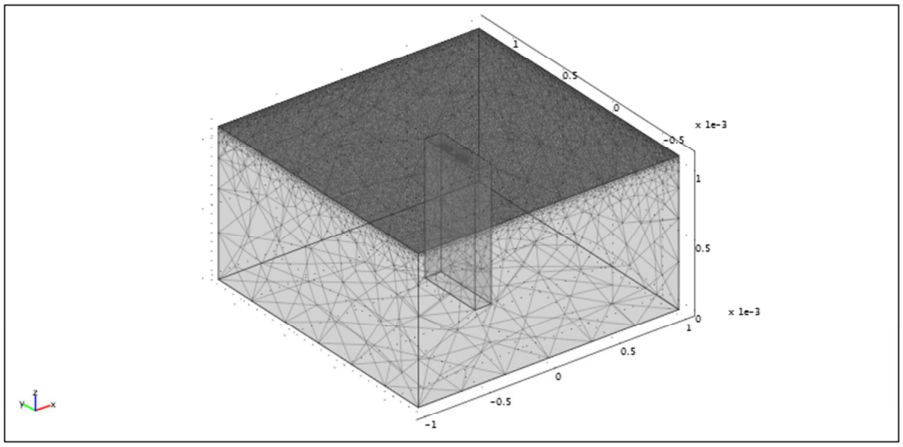

5.2. Application Mode: Convection and Diffusion (cd)

Application mode type: Convection and Diffusion

Application mode name: cd

5.2.1. Application Mode Properties

Property	**Value**
Default element type	Lagrange - Quadratic
Analysis type	Stationary
Equation form	Non-conservative
Frame	Frame (ref)
Weak constraints	Off
Constraint type	Ideal

5.2.2. Variables

Dependent variables: c

Shape functions: shlag(2,'c')

Interior boundaries not active

5.2.3. Boundary Settings

Boundary		1-3, 5, 15	4, 6-7, 9-10, 14	11
Type		Concentration	Insulation/Symmetry	Concentration
Concentration (c0)	mol/m^3	0	0	**c0**

Boundary		12	13
Type		Convective flux	Insulation/Symmetry
Concentration (c0)	mol/m^3	0	**c0**

5.2.4. Subdomain Settings

Subdomain		1
Diffusion coefficient (D)	m^2/s	**Diff**
x-velocity (u)	m/s	**u**
y-velocity (v)	m/s	**v**
z-velocity (w)	m/s	**w**

5.3. Application Mode: Incompressible Navier-Stokes (chns)

Application mode type: Incompressible Navier-Stokes (Chemical Engineering Module)

Application mode name: chns

5.3.1. Scalar Variables

Name	Variable	Value	Unit	Description
visc_vel_fact	visc_vel_fact_chns	10	1	Viscous velocity factor

5.3.2. Application Mode Properties

Property	**Value**
Default element type	Lagrange - P_2 P_1
Analysis type	Stationary
Corner smoothing	Off
Weakly compressible flow	Off
Turbulence model	None
Realizability	Off
Non-Newtonian flow	Off
Brinkman on by default	Off
Two-phase flow	Single-phase flow
Frame	Frame (ref)
Weak constraints	Off
Constraint type	Ideal

5.3.3. Variables

Dependent variables: u, v, w, p, logk, logd, logw, phi, psi, nxw, nyw, nzw

Shape functions: shlag(2,'u'), shlag(2,'v'), shlag(2,'w'), shlag(1,'p')

Interior boundaries not active

5.3.4. Boundary Settings

Boundary		1-3, 5, 15	4, 6-7, 9-10, 13-14	11
Type		Outlet	Wall	Inlet
outtype		Pressure, no viscous stress	Pressure, no viscous stress	Pressure, no viscous stress
Normal inflow velocity (U0in)	m/s	1	1	**linearFL**
Normal outflow velocity (U0out)	m/s	0	0	0

Boundary		12
Type		Outlet
outtype		**Velocity**
Normal inflow velocity (U0in)	m/s	1
Normal outflow velocity (U0out)	m/s	**linearFL2**

5.3.5. Subdomain Settings

Subdomain		1
Integration order (gporder)		**4 4 4 2**
Constraint order (cporder)		**2 2 2 1**
Density (rho)	kg/m^3	**rho**

Dynamic viscosity (eta)	Pa·s	**nu**

6. Solver Settings

Solve using a script: off

Analysis type	Stationary
Auto select solver	On
Solver	Stationary
Solution form	Automatic
Symmetric	Off
Adaptive mesh refinement	Off
Optimization/Sensitivity	Off
Plot while solving	Off

6.1. Direct (UMFPACK)

Solver type: Linear system solver

Parameter	**Value**
Pivot threshold	0.1
Memory allocation factor	0.7

6.2. Stationary

Parameter	**Value**

Linearity	Automatic
Relative tolerance	1.0E-8
Maximum number of iterations	50
Manual tuning of damping parameters	On
Highly nonlinear problem	On
Initial damping factor	1.0E-4
Minimum damping factor	1.0E-12
Restriction for step size update	10.0

6.3. Advanced

Parameter	**Value**
Constraint handling method	Elimination
Null-space function	Automatic
Automatic assembly block size	On
Assembly block size	1000
Use Hermitian transpose of constraint matrix and in symmetry detection	Off
Use complex functions with real input	Off
Stop if error due to undefined operation	On
Store solution on file	Off
Type of scaling	Automatic
Manual scaling	
Row equilibration	On

Manual control of reassembly	Off
Load constant	On
Constraint constant	On
Mass constant	On
Damping (mass) constant	On
Jacobian constant	On
Constraint Jacobian constant	On

7. Postprocessing

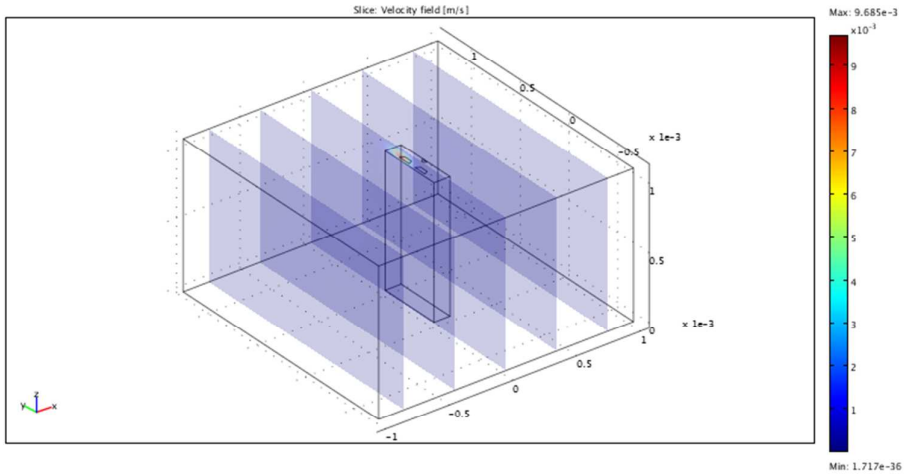

8. Variables

8.1. Boundary

8.1.1. Boundary 1-7, 9-15

Name	Description	Unit	Expression

ndflux_c_cd	Normal diffusive flux, c	mol/(m^2*s)	nx_cd * dflux_c_x_cd+ny_cd * dflux_c_y_cd+nz_cd * dflux_c_z_cd
ncflux_c_cd	Normal convective flux, c	mol/(m^2*s)	nx_cd * cflux_c_x_cd+ny_cd * cflux_c_y_cd+nz_cd * cflux_c_z_cd
ntflux_c_cd	Normal total flux, c	mol/(m^2*s)	nx_cd * tflux_c_x_cd+ny_cd * tflux_c_y_cd+nz_cd * tflux_c_z_cd
K_x_chns	Viscous force per area, x component	Pa	eta_chns * (2 * nx_chns * ux+ny_chns * (uy+vx)+nz_chns * (uz+wx))
T_x_chns	Total force per area, x component	Pa	-nx_chns * p+2 * nx_chns * eta_chns * ux+ny_chns * eta_chns * (uy+vx)+nz_chns * eta_chns * (uz+wx)
K_y_chns	Viscous force per area, y component	Pa	eta_chns * (nx_chns * (vx+uy)+2 * ny_chns * vy+nz_chns * (vz+wy))
T_y_chns	Total force per area, y component	Pa	-ny_chns * p+nx_chns * eta_chns * (vx+uy)+2 * ny_chns * eta_chns * vy+nz_chns * eta_chns * (vz+wy)
K_z_chns	Viscous force per area, z component	Pa	eta_chns * (nx_chns * (wx+uz)+ny_chns * (wy+vz)+2 * nz_chns * wz)
T_z_chns	Total force per area, z component	Pa	-nz_chns * p+nx_chns * eta_chns * (wx+uz)+ny_chns * eta_chns * (wy+vz)+2 * nz_chns * eta_chns * wz

8.1.2. Boundary 8

Name	Description	Unit	Expression

ndflux_c_cd	Normal diffusive flux, c	mol/(m^2*s)	
ncflux_c_cd	Normal convective flux, c	mol/(m^2*s)	
ntflux_c_cd	Normal total flux, c	mol/(m^2*s)	
K_x_chns	Viscous force per area, x component	Pa	
T_x_chns	Total force per area, x component	Pa	
K_y_chns	Viscous force per area, y component	Pa	
T_y_chns	Total force per area, y component	Pa	
K_z_chns	Viscous force per area, z component	Pa	
T_z_chns	Total force per area, z component	Pa	

8.2. Subdomain

8.2.1. Subdomain 1

Name	**Description**	**Unit**	**Expression**
grad_c_x_cd	Concentration gradient, c, x component	mol/m^4	cx
dflux_c_x_cd	Diffusive flux, c, x component	mol/(m^2*s)	-Dxx_c_cd * cx-Dxy_c_cd * cy-Dxz_c_cd * cz
cflux_c_x_cd	Convective flux, c, x component	mol/(m^2*s)	c * u_c_cd

tflux_c_x_cd	Total flux, c, x component	mol/(m^2*s)	dflux_c_x_cd+cflux_c_x_cd
grad_c_y_cd	Concentration gradient, c, y component	mol/m^4	cy
dflux_c_y_cd	Diffusive flux, c, y component	mol/(m^2*s)	-Dyx_c_cd * cx-Dyy_c_cd * cy-Dyz_c_cd * cz
cflux_c_y_cd	Convective flux, c, y component	mol/(m^2*s)	c * v_c_cd
tflux_c_y_cd	Total flux, c, y component	mol/(m^2*s)	dflux_c_y_cd+cflux_c_y_cd
grad_c_z_cd	Concentration gradient, c, z component	mol/m^4	cz
dflux_c_z_cd	Diffusive flux, c, z component	mol/(m^2*s)	-Dzx_c_cd * cx-Dzy_c_cd * cy-Dzz_c_cd * cz
cflux_c_z_cd	Convective flux, c, z	mol/(m^2*s)	c * w_c_cd

	component		
tflux_c_z_cd	Total flux, c, z component	mol/(m^2*s)	dflux_c_z_cd+cflux_c_z_cd
beta_c_x_cd	Convective field, c, x component	m/s	u_c_cd
beta_c_y_cd	Convective field, c, y component	m/s	v_c_cd
beta_c_z_cd	Convective field, c, z component	m/s	w_c_cd
grad_c_cd	Concentration gradient, c	mol/m^4	sqrt(grad_c_x_cd^2+grad_c_y_cd^2+grad_c_z_cd^2)
dflux_c_cd	Diffusive flux, c	mol/(m^2*s)	sqrt(dflux_c_x_cd^2+dflux_c_y_cd^2+dflux_c_z_cd^2)
cflux_c_cd	Convective flux, c	mol/(m^2*s)	sqrt(cflux_c_x_cd^2+cflux_c_y_cd^2+cflux_c_z_cd^2)
tflux_c_cd	Total flux, c	mol/(m^2*s)	sqrt(tflux_c_x_cd^2+tflux_c_y_cd^2+tflux_c_z_cd^2)
cellPe_c_cd	Cell Peclet number, c	1	h * sqrt(beta_c_x_cd^2+beta_c_y_cd^2+beta_c_z_cd^2)/D

			m_c_cd
Dm_c_cd	Mean diffusion coefficient, c	m^2/s	(Dxx_c_cd * u_c_cd^2+Dxy_c_cd * u_c_cd * v_c_cd+Dxz_c_cd * u_c_cd * w_c_cd+Dyx_c_cd * v_c_cd * u_c_cd+Dyy_c_cd * v_c_cd^2+Dyz_c_cd * v_c_cd * w_c_cd+Dzx_c_cd * w_c_cd * u_c_cd+Dzy_c_cd * w_c_cd * v_c_cd+Dzz_c_cd * w_c_cd^2)/(u_c_cd^2+v_c_cd^2+w_c_cd^2+eps)
res_c_cd	Equation residual for c	mol/(m^3*s)	-Dxx_c_cd * cxx-Dxy_c_cd * cxy-Dxz_c_cd * cxz+cx * u_c_cd-Dyx_c_cd * cyx-Dyy_c_cd * cyy-Dyz_c_cd * cyz+cy * v_c_cd-Dzx_c_cd * czx-Dzy_c_cd * czy-Dzz_c_cd * czz+cz * w_c_cd-R_c_cd
res_sc_c_cd	Shock capturing residual for c	mol/(m^3*s)	cx * u_c_cd+cy * v_c_cd+cz * w_c_cd-R_c_cd
da_c_cd	Total time scale factor, c	1	Dts_c_cd
U_chns	Velocity field	m/s	sqrt(u^2+v^2+w^2)
Vx_chns	Vorticity, x component	1/s	wy-vz
Vy_chns	Vorticity, y component	1/s	uz-wx

Vz_chns	Vorticity, z component	1/s	vx-uy
V_chns	Vorticity	1/s	sqrt(Vx_chns^2+Vy_chns^2+Vz_chns^2)
divU_chns	Divergence of velocity field	1/s	ux+vy+wz
cellRe_chns	Cell Reynolds number	1	rho_chns * U_chns * h/eta_chns
res_u_chns	Equation residual for u	N/m^3	rho_chns * (u * ux+v * uy+w * uz)+px-F_x_chns+if(gmg_level>0,0,-eta_chns * (2 * uxx+uyy+vxy+uzz+wxz))
res_v_chns	Equation residual for v	N/m^3	rho_chns * (u * vx+v * vy+w * vz)+py-F_y_chns+if(gmg_level>0,0,-eta_chns * (vxx+uyx+2 * vyy+vzz+wyz))
res_w_chns	Equation residual for w	N/m^3	rho_chns * (u * wx+v * wy+w * wz)+pz-F_z_chns+if(gmg_level>0,0,-eta_chns * (wxx+uzx+wyy+vzy+2 * wzz))
beta_x_chns	Convective field, x component	kg/(m^2*s)	rho_chns * u
beta_y_chns	Convective field, y component	kg/(m^2*s)	rho_chns * v

beta_z_chns	Convective field, z component	kg/(m^2*s)	rho_chns * w
Dm_chns	Mean diffusion coefficient	Pa*s	eta_chns
da_chns	Total time scale factor	kg/m^3	rho_chns
taum_chns	GLS time-scale	m^3*s/kg	nojac(1/max(2 * rho_chns * sqrt(emetric(u,v,w)),48 * eta_chns/h^2))
tauc_chns	GLS time-scale	m^2/s	0.5 * nojac(if(u^2+v^2+w^2<="" td="">
res_p_chns	Equation residual for p	kg/(m^3*s)	rho_chns * divU_chns

8.2.2. Subdomain 2

Name	Description	Unit	Expression
grad_c_x_cd	Concentration gradient, c, x component	mol/m^4	
dflux_c_x_cd	Diffusive flux, c, x component	mol/(m^2*s)	
cflux_c_x_cd	Convective flux, c, x component	mol/(m^2*s)	
tflux_c_x_cd	Total flux, c, x component	mol/(m^2*s)	
grad_c_y_cd	Concentration gradient, c, y component	mol/m^4	

dflux_c_y_cd	Diffusive flux, c, y component	mol/(m^2*s)	
cflux_c_y_cd	Convective flux, c, y component	mol/(m^2*s)	
tflux_c_y_cd	Total flux, c, y component	mol/(m^2*s)	
grad_c_z_cd	Concentration gradient, c, z component	mol/m^4	
dflux_c_z_cd	Diffusive flux, c, z component	mol/(m^2*s)	
cflux_c_z_cd	Convective flux, c, z component	mol/(m^2*s)	
tflux_c_z_cd	Total flux, c, z component	mol/(m^2*s)	
beta_c_x_cd	Convective field, c, x component	m/s	
beta_c_y_cd	Convective field, c, y component	m/s	
beta_c_z_cd	Convective field, c, z component	m/s	
grad_c_cd	Concentration gradient, c	mol/m^4	
dflux_c_cd	Diffusive flux, c	mol/(m^2*s)	
cflux_c_cd	Convective flux, c	mol/(m^2*s)	
tflux_c_cd	Total flux, c	mol/(m^2*s)	
cellPe_c_cd	Cell Peclet number, c	1	
Dm_c_cd	Mean diffusion coefficient, c	m^2/s	
res_c_cd	Equation residual for c	mol/(m^3*s)	
res_sc_c_cd	Shock capturing residual for c	mol/(m^3*s)	
da_c_cd	Total time scale factor, c	1	
U_chns	Velocity field	m/s	
Vx_chns	Vorticity, x component	1/s	
Vy_chns	Vorticity, y component	1/s	

Vz_chns	Vorticity, z component	1/s	
V_chns	Vorticity	1/s	
divU_chns	Divergence of velocity field	1/s	
cellRe_chns	Cell Reynolds number	1	
res_u_chns	Equation residual for u	N/m^3	
res_v_chns	Equation residual for v	N/m^3	
res_w_chns	Equation residual for w	N/m^3	
beta_x_chns	Convective field, x component	kg/(m^2*s)	
beta_y_chns	Convective field, y component	kg/(m^2*s)	
beta_z_chns	Convective field, z component	kg/(m^2*s)	
Dm_chns	Mean diffusion coefficient	Pa*s	
da_chns	Total time scale factor	kg/m^3	
taum_chns	GLS time-scale	m^3*s/kg	
tauc_chns	GLS time-scale	m^2/s	
res_p_chns	Equation residual for p	kg/(m^3*s)	

SI-IV. Numerical simulation for the electrochemical push-pull probe operated in the electrochemical mode.

The electrochemical operation mode of the electrochemical push-pull probe is based on the *in situ* electrochemical generation of species that can perturb adherent cells locally, *e.g.* the non-active compound A, present in the solution, is converted into an active compound B at the electrode *via* its electrochemical reduction:

$$A + n\mathrm{e}^- \xrightarrow{k} B$$

where n corresponds to the number of electrons transferred. For the numerical simulations a fast kinetic rate constant (*i.e.* $k = 10^6$ m×s^{-1}) was assumed. To simulate the distribution of the compound B over the sample surface, the Fick's second law in steady-state conditions has to be solved:

$$\nabla \cdot (-D\nabla c_A) = 0 \tag{S5}$$

where D is the diffusion coefficient and c_A is the concentration of the compound A at a given time. The values of the parameters used for the simulations are given in Table S5.

Table S5. The values of the parameters used for the simulations of the electrochemical mode

Parameter	Value [units]	Name
D	1×10^{-9} [m^2/s]	diffusion coefficient
c_0	1 [mol/L]	initial concentration of cpmpound A
k	1×10^{6} [m/s]	kinetic rate constant at microelectrode

The boundary conditions listed in Table S6 were employed to solve the present model.

Table S6. The boundary conditions for the differential equation S5. Herein, $\boldsymbol{n}$ is the vector normal to the surface.

Surface	**Diffusion of A**
Active surface of electrode	Concentration; $c_A = 0$
Body of the probe	Insulation/Symmetry; $\boldsymbol{n} \cdot (-D\nabla c_A) = 0$
Box planes (except reactive pattern)	Concentration; $c_A = c_0$; $c_0 = 1\ M$
Substrate pattern	Insulation/Symmetry; $\boldsymbol{n} \cdot (-D\nabla c_A) = 0$
Pushing microchannel	Insulation/Symmetry; $\boldsymbol{n} \cdot (-D\nabla c_A) = 0$
Aspirating microchannel	Insulation/Symmetry; $\boldsymbol{n} \cdot (-D\nabla c_A) = 0$

The results of the numerical simulations are presented in Figure S6, Figure S7 and in the main manuscript.

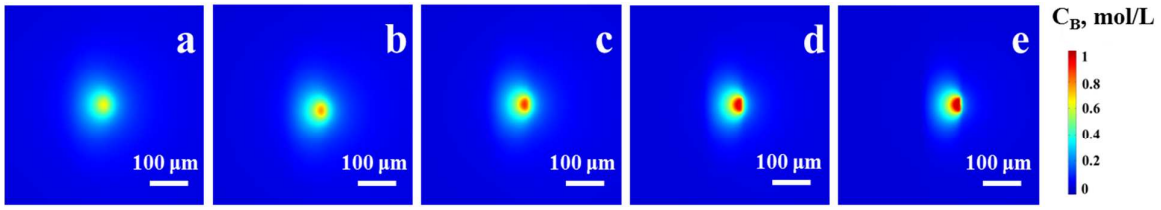

Figure S6. Simulated concentration profiles of the active compound B on the sample surface generated by the electrochemical push-pull probe operated in an electrochemical mode. The inclination angle was equal to 90° and the working distance *d* was: a) 20 µm; b) 15 µm; c) 10 µm; d) 5 µm; e) 2 µm.

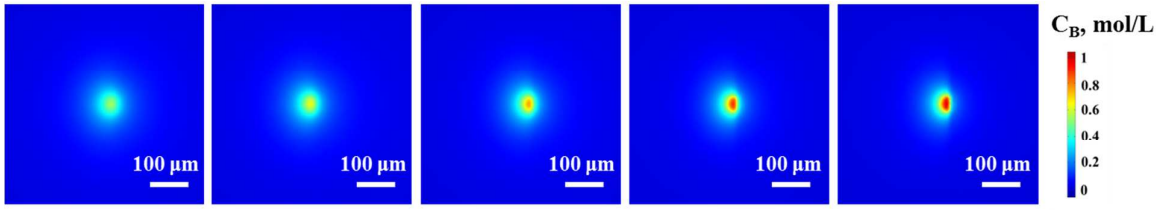

Figure S7. Simulated concentration profiles of the active compound B on the sample surface generated by the electrochemical push-pull probe operated in an electrochemical mode. The inclination angle was equal to 70° and the working distance *d* was: a) 20 µm; b) 15 µm; c) 10 µm; d) 5 µm; e) 2 µm.

The numerical simulations indicated a non-significant influence of the inclination angle on the affected area and the behavior of the system in general. However, the working distance has a significant influence on the concentration profile of the active compound B over the substrate and on the whole affected area. For more details see Results and discussion, Computational model and numerical simulations.

Typical COMSOL Model Report for the simulations of Convection-Diffusion equation. The working distance *d* was equal to 2 μm and the inclination angle was equal to 70°.

COMSOL Model Report

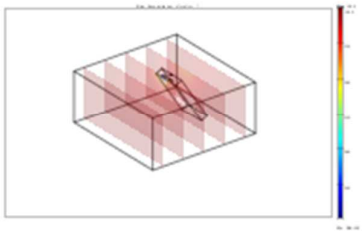

1. Table of Contents

2. Model Properties

Property	**Value**
Model name	
Author	
Company	

Department	
Reference	
URL	
Saved date	Mar 17, 2015 5:26:58 PM
Creation date	Nov 20, 2012 10:02:44 AM
COMSOL version	COMSOL 3.5.0.603

File name: /home/dmitry/Desktop/Alexandra/Corrections/Elchem_example.mph

Application modes and modules used in this model:

- Geom1 (3D)
    - Convection and Diffusion
    - Incompressible Navier-Stokes (Chemical Engineering Module)

3. Constants

Name	Expression	Value	Description
rho	1000[kg/m^3]		density of water
nu	8.94e-4[Pa*s]		water viscosity
Diff	1e-9[m^2/s]		diffusion coefficient for analyte
c0	1[mol/L]		initial analyte concentration
k1	1e6[m/s]		kinetic rate constant

4. Geometry

Number of geometries: 1

4.1. Geom1

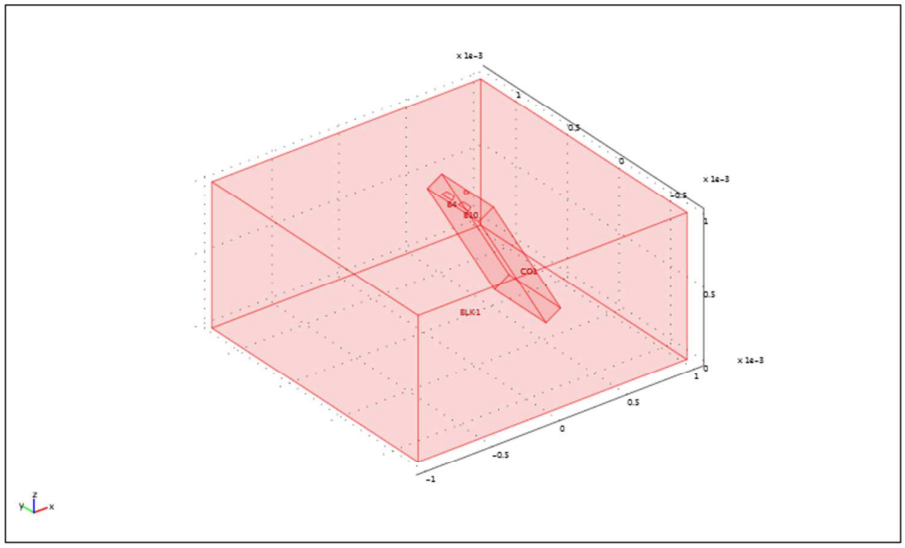

4.1.1. Point mode

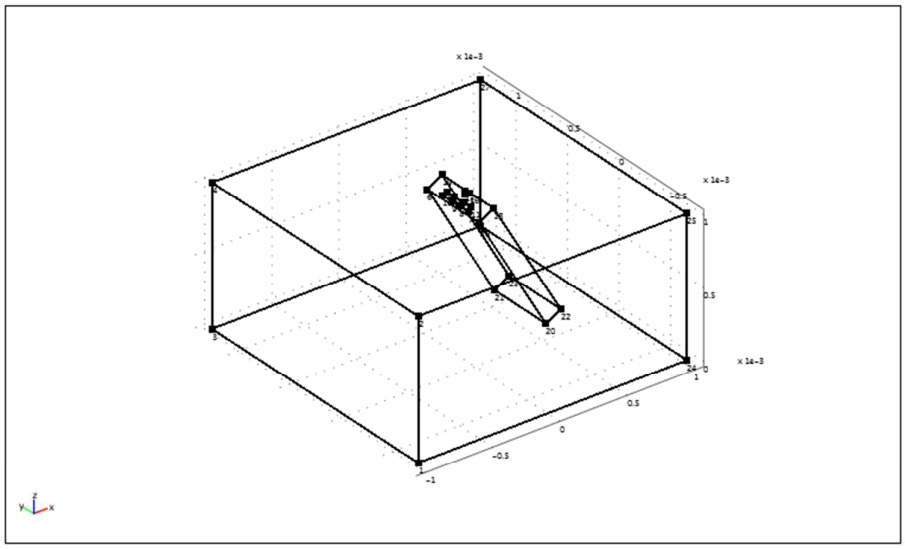

4.1.2. Edge mode

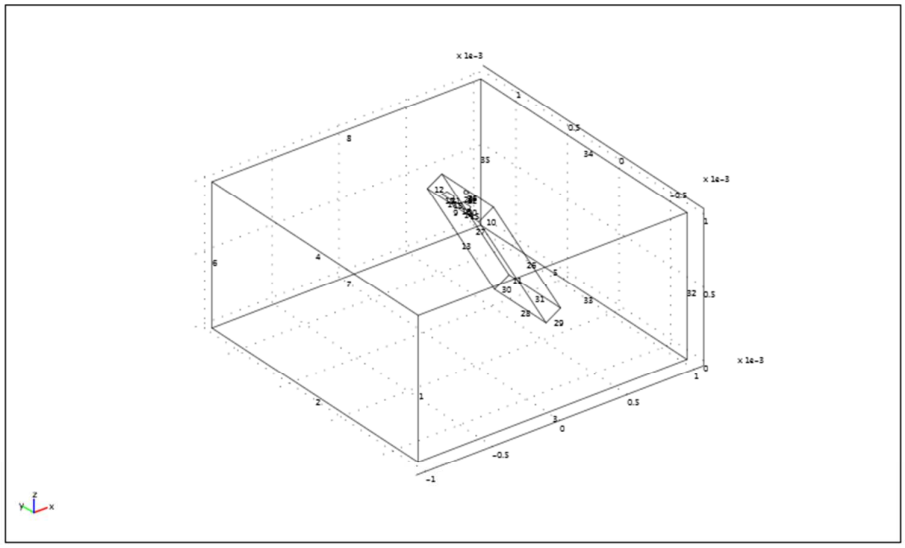

4.1.3. Boundary mode

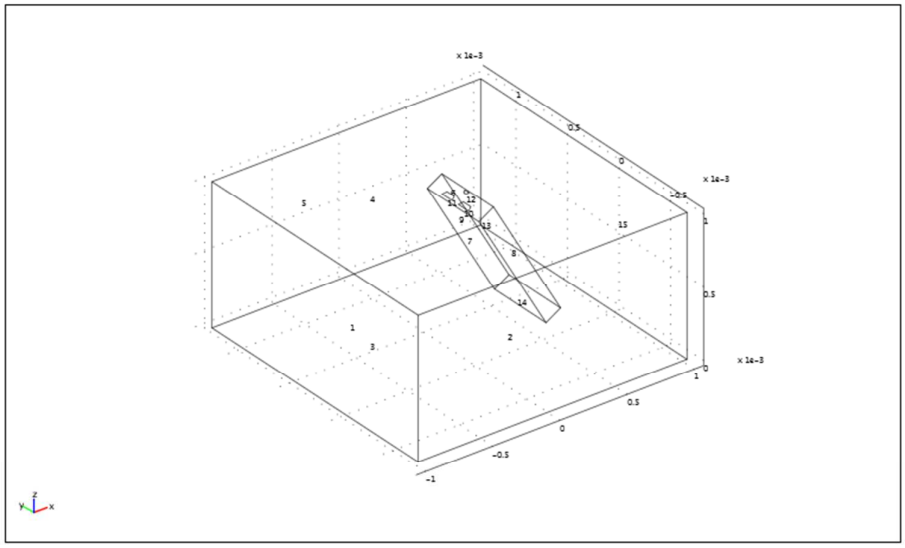

4.1.4. Subdomain mode

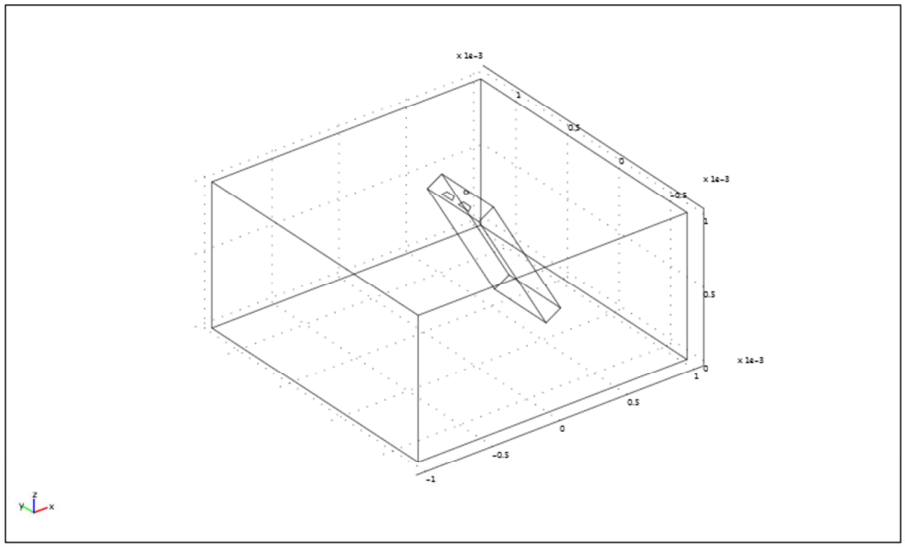

5. Geom1

Space dimensions: 3D

Independent variables: x, y, z

5.1. Mesh

5.1.1. Mesh Statistics

Number of degrees of freedom	1620430
Number of mesh points	62209
Number of elements	309675
Tetrahedral	309675
Prism	0
Hexahedral	0
Number of boundary elements	50010

Triangular	50010
Quadrilateral	0
Number of edge elements	1007
Number of vertex elements	27
Minimum element quality	0.032
Element volume ratio	0

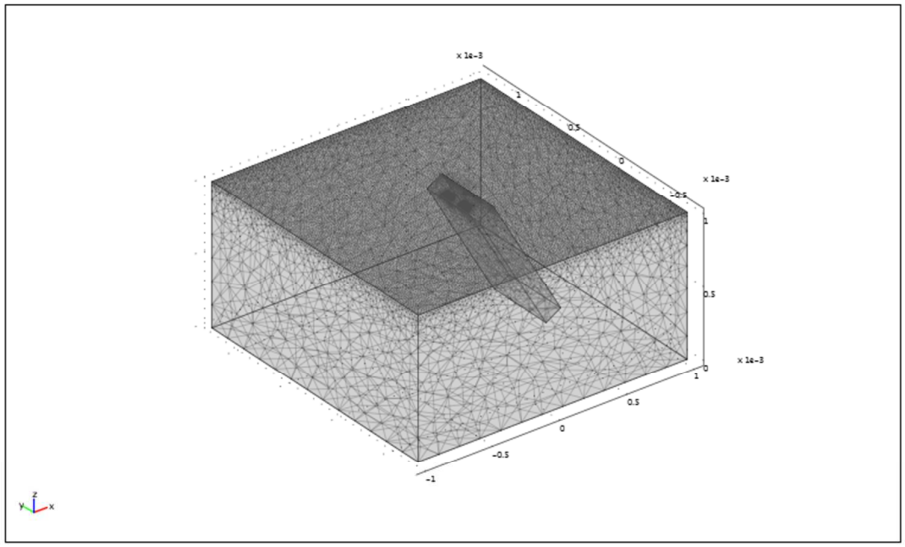

5.2. Application Mode: Convection and Diffusion (cd)

Application mode type: Convection and Diffusion

Application mode name: cd

5.2.1. Application Mode Properties

Property	**Value**

Default element type	Lagrange - Quadratic
Analysis type	Stationary
Equation form	Non-conservative
Frame	Frame (ref)
Weak constraints	Off
Constraint type	Ideal

5.2.2. Variables

Dependent variables: c

Shape functions: shlag(2,'c')

Interior boundaries not active

5.2.3. Boundary Settings

Boundary		12	4, 6-9, 11, 13	1-3, 5, 10, 14-15
Type		Concentration	Insulation/Symmetry	Concentration
Concentration (c0)	mol/m^3	0	0	**c0**

5.2.4. Subdomain Settings

Subdomain		1
Diffusion coefficient (D)	m^2/s	**Diff**
Subdomain initial value		1
Concentration, c (c)	mol/m^3	c0

5.3. Application Mode: Incompressible Navier-Stokes (chns)

Application mode type: Incompressible Navier-Stokes (Chemical Engineering Module)

Application mode name: chns

5.3.1. Scalar Variables

Name	Variable	Value	Unit	Description
visc_vel_fact	visc_vel_fact_chns	10	1	Viscous velocity factor

5.3.2. Application Mode Properties

Property	**Value**
Default element type	Lagrange - P_2 P_1
Analysis type	Stationary
Corner smoothing	Off
Weakly compressible flow	Off
Turbulence model	None
Realizability	Off
Non-Newtonian flow	Off
Brinkman on by default	Off
Two-phase flow	Single-phase flow
Frame	Frame (ref)
Weak constraints	Off
Constraint type	Ideal

5.3.3. Variables

Dependent variables: u, v, w, p, logk, logd, logw, phi, psi, nxw, nyw, nzw

Shape functions: shlag(2,'u'), shlag(2,'v'), shlag(2,'w'), shlag(1,'p')

Interior boundaries not active

5.3.4. Boundary Settings

Boundary		1-3, 5, 15	4, 6-9, 12-14	10
Type		Outlet	Wall	Inlet
outtype		Pressure, no viscous stress	Pressure, no viscous stress	Pressure, no viscous stress
Normal inflow velocity (U0in)	m/s	1	1	**linearFL**
Normal outflow velocity (U0out)	m/s	0	0	0

Boundary		11
Type		Outlet
outtype		**Velocity**
Normal inflow velocity (U0in)	m/s	1
Normal outflow velocity (U0out)	m/s	**linearFL2**

5.3.5. Subdomain Settings

Subdomain		1
Integration order (gporder)		**4 4 4 2**

Constraint order (cporder)		**2 2 2 1**
Density (rho)	kg/m^3	**rho**
Dynamic viscosity (eta)	Pa·s	**nu**

6. Solver Settings

Solve using a script: off

Analysis type	Stationary
Auto select solver	On
Solver	Stationary
Solution form	Automatic
Symmetric	Off
Adaptive mesh refinement	Off
Optimization/Sensitivity	Off
Plot while solving	Off

6.1. Direct (UMFPACK)

Solver type: Linear system solver

Parameter	**Value**
Pivot threshold	0.1
Memory allocation factor	0.7

6.2. Stationary

Parameter	Value
Linearity	Automatic
Relative tolerance	1.0E-8
Maximum number of iterations	25
Manual tuning of damping parameters	On
Highly nonlinear problem	On
Initial damping factor	1.0E-4
Minimum damping factor	1.0E-12
Restriction for step size update	10.0

6.3. Advanced

Parameter	Value
Constraint handling method	Elimination
Null-space function	Automatic
Automatic assembly block size	On
Assembly block size	1000
Use Hermitian transpose of constraint matrix and in symmetry detection	Off
Use complex functions with real input	Off
Stop if error due to undefined operation	On
Store solution on file	Off
Type of scaling	Automatic
Manual scaling	

Row equilibration	On
Manual control of reassembly	Off
Load constant	On
Constraint constant	On
Mass constant	On
Damping (mass) constant	On
Jacobian constant	On
Constraint Jacobian constant	On

7. Postprocessing

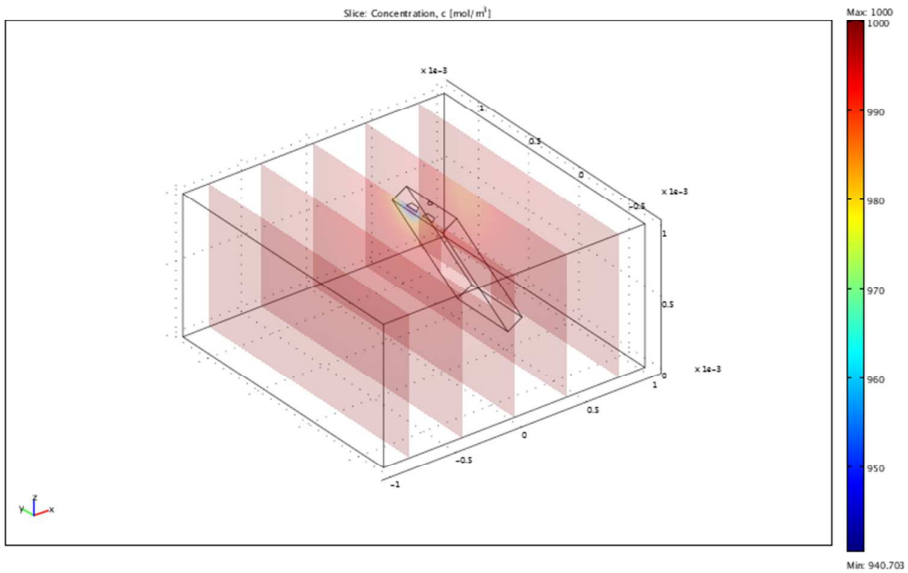

8. Variables

8.1. Boundary

Name	Description	Unit	Expression

ndflux_c_cd	Normal diffusive flux, c	mol/(m^2*s)	nx_cd * dflux_c_x_cd+ny_cd * dflux_c_y_cd+nz_cd * dflux_c_z_cd
ncflux_c_cd	Normal convective flux, c	mol/(m^2*s)	nx_cd * cflux_c_x_cd+ny_cd * cflux_c_y_cd+nz_cd * cflux_c_z_cd
ntflux_c_cd	Normal total flux, c	mol/(m^2*s)	nx_cd * tflux_c_x_cd+ny_cd * tflux_c_y_cd+nz_cd * tflux_c_z_cd
K_x_chns	Viscous force per area, x component	Pa	eta_chns * (2 * nx_chns * ux+ny_chns * (uy+vx)+nz_chns * (uz+wx))
T_x_chns	Total force per area, x component	Pa	-nx_chns * p+2 * nx_chns * eta_chns * ux+ny_chns * eta_chns * (uy+vx)+nz_chns * eta_chns * (uz+wx)
K_y_chns	Viscous force per area, y component	Pa	eta_chns * (nx_chns * (vx+uy)+2 * ny_chns * vy+nz_chns * (vz+wy))
T_y_chns	Total force per area, y component	Pa	-ny_chns * p+nx_chns * eta_chns * (vx+uy)+2 * ny_chns * eta_chns * vy+nz_chns * eta_chns * (vz+wy)
K_z_chns	Viscous force per area, z component	Pa	eta_chns * (nx_chns * (wx+uz)+ny_chns * (wy+vz)+2 * nz_chns * wz)
T_z_chns	Total force per area, z component	Pa	-nz_chns * p+nx_chns * eta_chns * (wx+uz)+ny_chns * eta_chns * (wy+vz)+2 * nz_chns * eta_chns * wz

8.2. Subdomain

8.2.1. Subdomain 1

Name	Description	Unit	Expression

grad_c_x_cd	Concentration gradient, c, x component	mol/m^4	cx
dflux_c_x_cd	Diffusive flux, c, x component	mol/(m^2*s)	-Dxx_c_cd * cx-Dxy_c_cd * cy-Dxz_c_cd * cz
cflux_c_x_cd	Convective flux, c, x component	mol/(m^2*s)	c * u_c_cd
tflux_c_x_cd	Total flux, c, x component	mol/(m^2*s)	dflux_c_x_cd+cflux_c_x_cd
grad_c_y_cd	Concentration gradient, c, y component	mol/m^4	cy
dflux_c_y_cd	Diffusive flux, c, y component	mol/(m^2*s)	-Dyx_c_cd * cx-Dyy_c_cd * cy-Dyz_c_cd * cz
cflux_c_y_cd	Convective flux, c, y component	mol/(m^2*s)	c * v_c_cd
tflux_c_y_cd	Total flux, c, y	mol/(m^2*s)	dflux_c_y_cd+cflux_c_y_cd

	component		
grad_c_z_cd	Concentration gradient, c, z component	mol/m^4	cz
dflux_c_z_cd	Diffusive flux, c, z component	mol/(m^2*s)	-Dzx_c_cd * cx-Dzy_c_cd * cy-Dzz_c_cd * cz
cflux_c_z_cd	Convective flux, c, z component	mol/(m^2*s)	c * w_c_cd
tflux_c_z_cd	Total flux, c, z component	mol/(m^2*s)	dflux_c_z_cd+cflux_c_z_cd
beta_c_x_cd	Convective field, c, x component	m/s	u_c_cd
beta_c_y_cd	Convective field, c, y component	m/s	v_c_cd
beta_c_z_cd	Convective field, c, z component	m/s	w_c_cd
grad_c_cd	Concentrati	mol/m^4	sqrt(grad_c_x_cd^2+grad_c_y_cd^2+grad_c_z_cd^2)

	on gradient, c		
dflux_c_cd	Diffusive flux, c	mol/(m^2*s)	sqrt(dflux_c_x_cd^2+dflux_c_y_cd^2+dflux_c_z_cd^2)
cflux_c_cd	Convective flux, c	mol/(m^2*s)	sqrt(cflux_c_x_cd^2+cflux_c_y_cd^2+cflux_c_z_cd^2)
tflux_c_cd	Total flux, c	mol/(m^2*s)	sqrt(tflux_c_x_cd^2+tflux_c_y_cd^2+tflux_c_z_cd^2)
cellPe_c_cd	Cell Peclet number, c	1	h * sqrt(beta_c_x_cd^2+beta_c_y_cd^2+beta_c_z_cd^2)/Dm_c_cd
Dm_c_cd	Mean diffusion coefficient, c	m^2/s	(Dxx_c_cd * u_c_cd^2+Dxy_c_cd * u_c_cd * v_c_cd+Dxz_c_cd * u_c_cd * w_c_cd+Dyx_c_cd * v_c_cd * u_c_cd+Dyy_c_cd * v_c_cd^2+Dyz_c_cd * v_c_cd * w_c_cd+Dzx_c_cd * w_c_cd * u_c_cd+Dzy_c_cd * w_c_cd * v_c_cd+Dzz_c_cd * w_c_cd^2)/(u_c_cd^2+v_c_cd^2+w_c_cd^2+eps)
res_c_cd	Equation residual for c	mol/(m^3*s)	-Dxx_c_cd * cxx-Dxy_c_cd * cxy-Dxz_c_cd * cxz+cx * u_c_cd-Dyx_c_cd * cyx-Dyy_c_cd * cyy-Dyz_c_cd * cyz+cy * v_c_cd-Dzx_c_cd * czx-Dzy_c_cd * czy-Dzz_c_cd * czz+cz * w_c_cd-R_c_cd
res_sc_c_cd	Shock capturing residual for c	mol/(m^3*s)	cx * u_c_cd+cy * v_c_cd+cz * w_c_cd-R_c_cd

da_c_cd	Total time scale factor, c	1	Dts_c_cd
U_chns	Velocity field	m/s	sqrt(u^2+v^2+w^2)
Vx_chns	Vorticity, x component	1/s	wy-vz
Vy_chns	Vorticity, y component	1/s	uz-wx
Vz_chns	Vorticity, z component	1/s	vx-uy
V_chns	Vorticity	1/s	sqrt(Vx_chns^2+Vy_chns^2+Vz_chns^2)
divU_chns	Divergence of velocity field	1/s	ux+vy+wz
cellRe_chns	Cell Reynolds number	1	rho_chns * U_chns * h/eta_chns
res_u_chns	Equation residual for u	N/m^3	rho_chns * (u * ux+v * uy+w * uz)+px-F_x_chns+if(gmg_level>0,0,-eta_chns * (2 * uxx+uyy+vxy+uzz+wxz))
res_v_chns	Equation residual for v	N/m^3	rho_chns * (u * vx+v * vy+w * vz)+py-F_y_chns+if(gmg_level>0,0,-eta_chns * (vxx+uyx+2 * vyy+vzz+wyz))

res_w_chns	Equation residual for w	N/m^3	rho_chns * (u * wx+v * wy+w * wz)+pz-F_z_chns+if(gmg_level>0,0,-eta_chns * (wxx+uzx+wyy+vzy+2 * wzz))
beta_x_chns	Convective field, x component	kg/(m^2*s)	rho_chns * u
beta_y_chns	Convective field, y component	kg/(m^2*s)	rho_chns * v
beta_z_chns	Convective field, z component	kg/(m^2*s)	rho_chns * w
Dm_chns	Mean diffusion coefficient	Pa*s	eta_chns
da_chns	Total time scale factor	kg/m^3	rho_chns
taum_chns	GLS time-scale	m^3*s/kg	nojac(1/max(2 * rho_chns * sqrt(emetric(u,v,w)),48 * eta_chns/h^2))
tauc_chns	GLS time-scale	m^2/s	0.5 * nojac(if(u^2+v^2+w^2<="" td="">
res_p_chns	Equation residual for p	kg/(m^3*s)	rho_chns * divU_chns

8.2.2. Subdomain 2

Name	Description	Unit	Expression
grad_c_x_cd	Concentration gradient, c, x component	mol/m^4	
dflux_c_x_cd	Diffusive flux, c, x component	mol/(m^2*s)	
cflux_c_x_cd	Convective flux, c, x component	mol/(m^2*s)	
tflux_c_x_cd	Total flux, c, x component	mol/(m^2*s)	
grad_c_y_cd	Concentration gradient, c, y component	mol/m^4	
dflux_c_y_cd	Diffusive flux, c, y component	mol/(m^2*s)	
cflux_c_y_cd	Convective flux, c, y component	mol/(m^2*s)	
tflux_c_y_cd	Total flux, c, y component	mol/(m^2*s)	
grad_c_z_cd	Concentration gradient, c, z component	mol/m^4	
dflux_c_z_cd	Diffusive flux, c, z component	mol/(m^2*s)	
cflux_c_z_cd	Convective flux, c, z component	mol/(m^2*s)	
tflux_c_z_cd	Total flux, c, z component	mol/(m^2*s)	
beta_c_x_cd	Convective field, c, x component	m/s	
beta_c_y_cd	Convective field, c, y component	m/s	
beta_c_z_cd	Convective field, c, z component	m/s	
grad_c_cd	Concentration gradient, c	mol/m^4	
dflux_c_cd	Diffusive flux, c	mol/(m^2*s)	
cflux_c_cd	Convective flux, c	mol/(m^2*s)	
tflux_c_cd	Total flux, c	mol/(m^2*s)	
cellPe_c_cd	Cell Peclet number, c	1	

Dm_c_cd	Mean diffusion coefficient, c	m^2/s	
res_c_cd	Equation residual for c	mol/(m^3*s)	
res_sc_c_cd	Shock capturing residual for c	mol/(m^3*s)	
da_c_cd	Total time scale factor, c	1	
U_chns	Velocity field	m/s	
Vx_chns	Vorticity, x component	1/s	
Vy_chns	Vorticity, y component	1/s	
Vz_chns	Vorticity, z component	1/s	
V_chns	Vorticity	1/s	
divU_chns	Divergence of velocity field	1/s	
cellRe_chns	Cell Reynolds number	1	
res_u_chns	Equation residual for u	N/m^3	
res_v_chns	Equation residual for v	N/m^3	
res_w_chns	Equation residual for w	N/m^3	
beta_x_chns	Convective field, x component	kg/(m^2*s)	
beta_y_chns	Convective field, y component	kg/(m^2*s)	
beta_z_chns	Convective field, z component	kg/(m^2*s)	
Dm_chns	Mean diffusion coefficient	Pa*s	
da_chns	Total time scale factor	kg/m^3	
taum_chns	GLS time-scale	m^3*s/kg	
tauc_chns	GLS time-scale	m^2/s	
res_p_chns	Equation residual for p	kg/(m^3*s)	

SI-V. Delivery of AO by the electrochemical push-pull probe operated in the microfluidic mode.

For the microfluidic experiments AO was only delivered during the first 2 min, while the aspiration rate was kept constant along the complete duration of the experiment (*i.e.* 10 min). After the delivery process was activated, the area of fluorescent labeled cells grew progressively (Figure S8a - f), until a steady-state condition was reached (Figure S8g - j, *i.e.* after 60 s from starting the experiment).

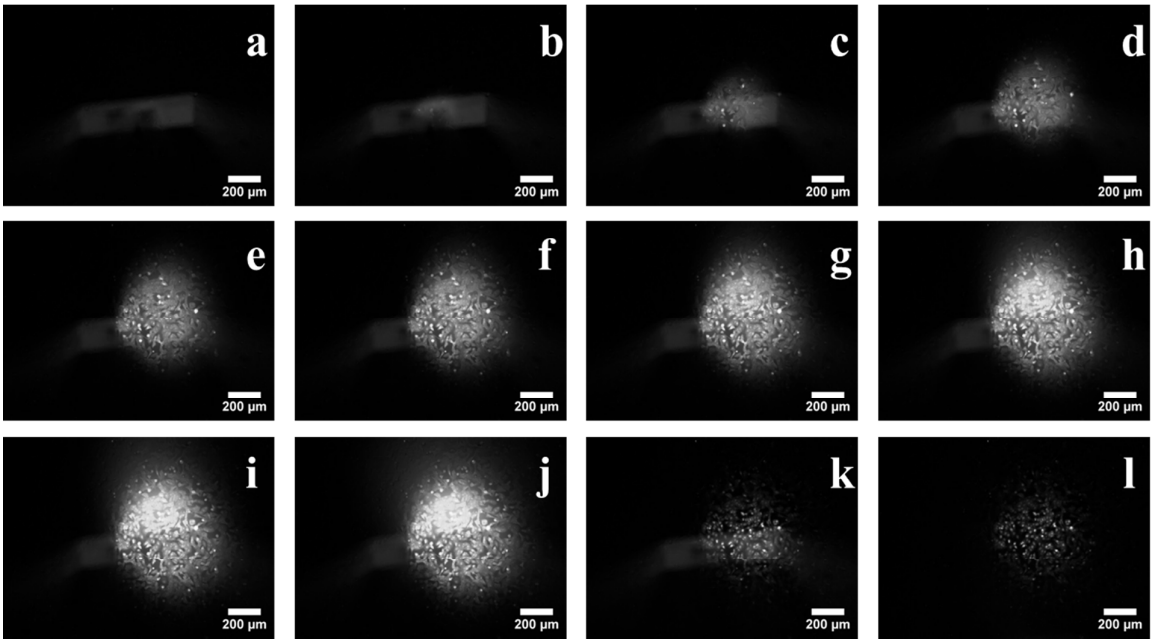

Figure S8. Evolution of affected area of cells as a function of time when the electrochemical push-pull probe is operated in a microfluidic mode. a) to j) shows fluorescence microscopy images of the cell surface taken 10 s from each other, or k) 500 s after the AO delivery started and l) is the final image after removing the probe from observed area. The inclination angle was equal to 70°, the working distance was 100 µm, the nominal pushing and aspirating flow rates were 1 µL/min and 20 µL/min, respectively.

After 500 s the intensity of the fluorescence decreased drastically most likely due to aspiration or partially diffusion away of the remaining AO in the solution as the pushing channel was stopped 120 s after the experiment was started (Figure S8k). As a result, the real affected area can be more clearly observed at times longer than 500 s. It is worth noticing that both a constant decrease of the AO fluorescence as well as a pronounced autofluorescence of the probe body (*i.e.* PET and PE) were observed during all the experiments. To overcome such situation, a precise time control of the cell perturbation was followed by the displacement of the probe from the field

of view of the microscope before the final image of the perturbed cells was obtained (Figure S8l).

SI-VI. Experimental verification for the electrochemical push-pull probe operated in the microfluidic mode.

The electrochemical push-pull probe in the microfluidic mode was applied to label adherent A549 cancer cells with AO using a pre-defined inclination angle of the probe (*i.e.* 90° or 70°) and probe-cells distance (*e.g.* 50 µm, 100 µm or 250 µm) with and without aspiration.

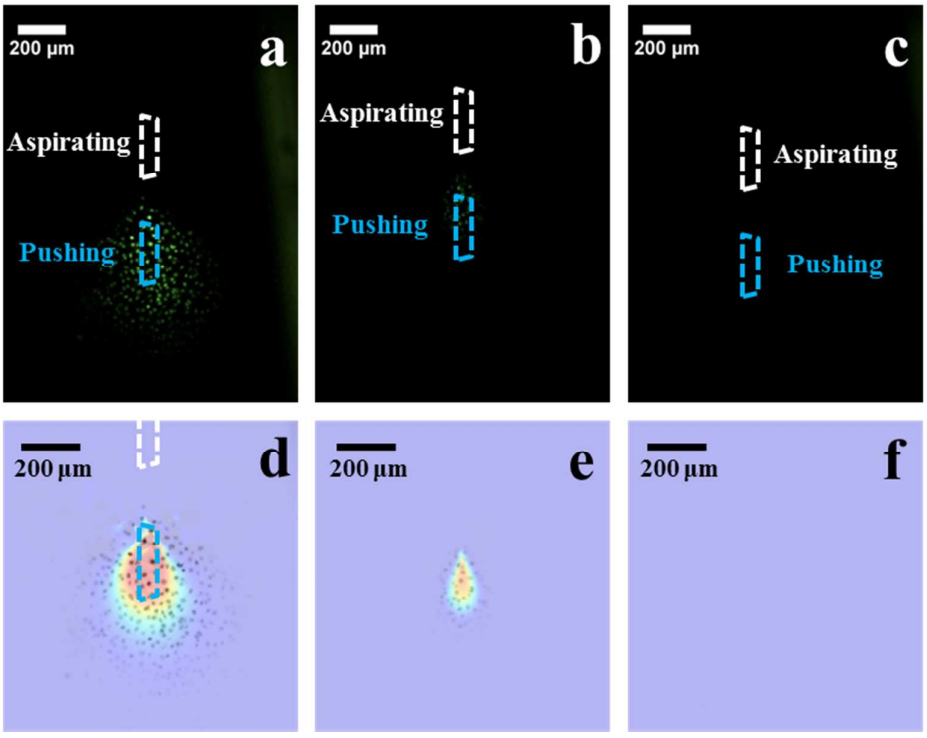

Figure S9. a) to c) Fluorescence microscopy images of the cancer cells surface affected by the electrochemical push-pull probe operated in a microfluidic mode. Blue and white dash lines correspond to the position of the pushing and aspirating microchannels, respectively. d) to f) depict the overlapping between the numerically simulated affected area (color image) and the experimental results (black-and-white image). The experimental nominal aspirating flow rate was 20 µL/min, while the one used for the simulations was 10 µL/min. The working distance *d* was: a) and d) 50 µm; b) and e) 100 µm; c) and f) 250 µm. The pushing flow rate was 1 µL/min and the inclination angle was equal to 90° for all experiments.

The most representative experimentally obtained results are presented in Figure S9 and Figure 5 of the main manuscript. As it can be seen in these figures, a good agreement between the experimentally observed behavior in terms of shape and size of the affected area and the numerical results was observed (especially when it comes to the effect of the working distance and inclination angle on the affected area). Based on the working distance and the obtained affected area, the effective experimental aspirating flow rate should be close to 10 µL/min and 3 µL/min for 90° and 70° inclination angle positioning, respectively.

SI-VII. Influence of basic pH on the fluorescence of acridine orange.

Electrolysis of water was carried out at the integrated carbon UME that was positioned above AO-labeled cells to decrease the fluorescence intensity of the AO-labeled cells. To prove that this phenomenon is due to the effect of basic pH on the fluorescence of AO, we have evaluated the emission spectra of Ringer solutions with 0.2% AO and three different pH values. As shown in Figure S10, the AO emission spectra (measured with a Jasco 750 spectrofluorimeter using 480 nm excitation wavelength) reveal a decrease of the fluorescence intensity as the pH of the media increases.

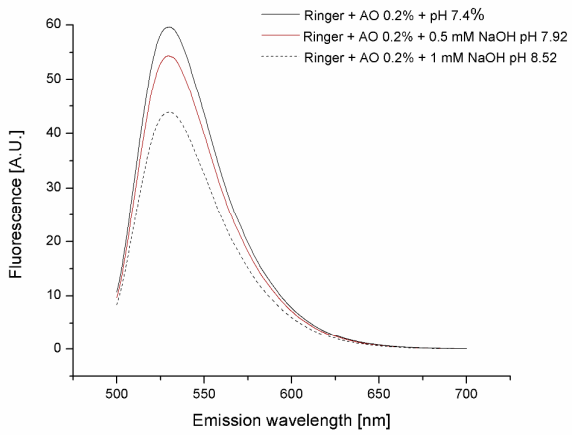

Figure S10. Fluorescent emission spectra of a solution of 0.2% AO in Ringer buffer at different pH values.

To further confirm that the fluorescence intensity of the AO labeled cells is indeed decreased by a local, electrochemically induced increase of pH, a 0.01 M NaOH solution was delivered from the probe over previously AO labeled adherent cells. As it is observed in Figure S11, the fluorescence of the labeled cells is drastically decreased by the presence of NaOH, as it was also observed when an extreme negative potential was applied at the UME (see Figure 6 of the main manuscript). Moreover, after the delivery of the basic solution was stopped, cells on the border of the affected area recovered their fluorescence, as shown in Figure S11. However, for the cells located just below the NaOH delivery zone, slight or negligible recovery was observed most likely due to the longer exposure to a high NaOH concentration that can irreversibly affect the pH cell status.

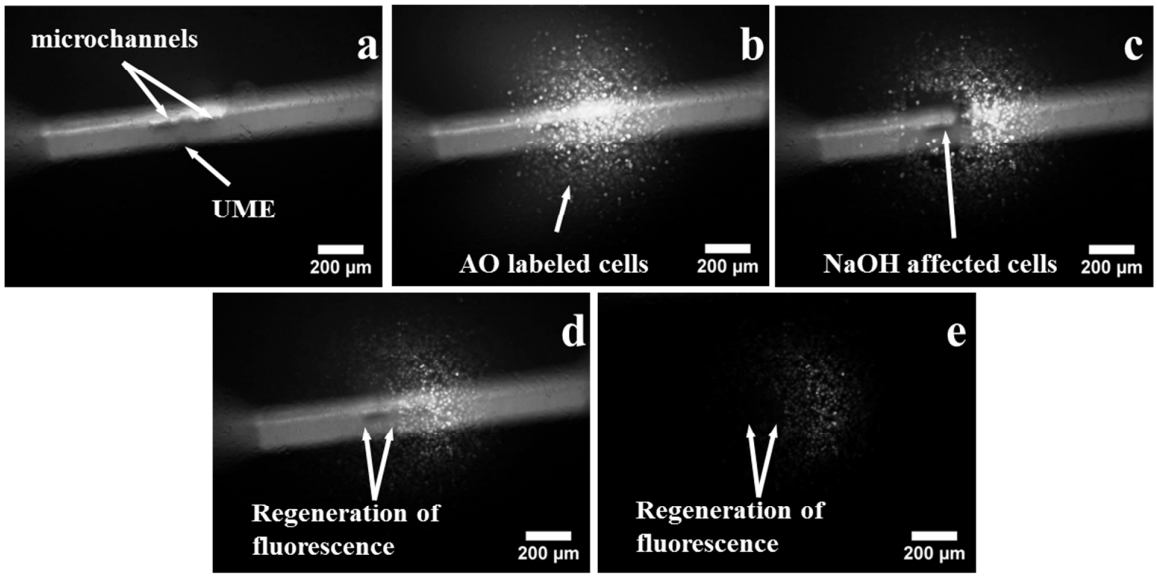

Figure S11. Fluorescence microscopy images of adherent cancer cells a) after the electrochemical push-pull probe is positioned above them, b) after pushing of AO with a flow rate of 1 µL/min during 50 s, c) after pushing of 0.01 M NaOH with a flow rate 0.5 µL/min during 50 s, d) 5 min after NaOH flow was stopped and e) after moving the probe outside the view.

SI-VIII. Experimental verification for the electrochemical push-pull probe operated in the electrochemical mode.

The electrochemical push-pull probe in the electrochemical mode and with pre-defined inclination angle (*i.e.* 90° or 70°) and working distance (*e.g.* 2 µm, 10 µm, 15 µm or 20 µm) was applied to quench the fluorescence of AO labeled adherent A549 cancer cells. The main results obtained for the perturbation of adherent cells with the probe operating in an electrochemical mode are shown in Figure S12 and Figure S13.

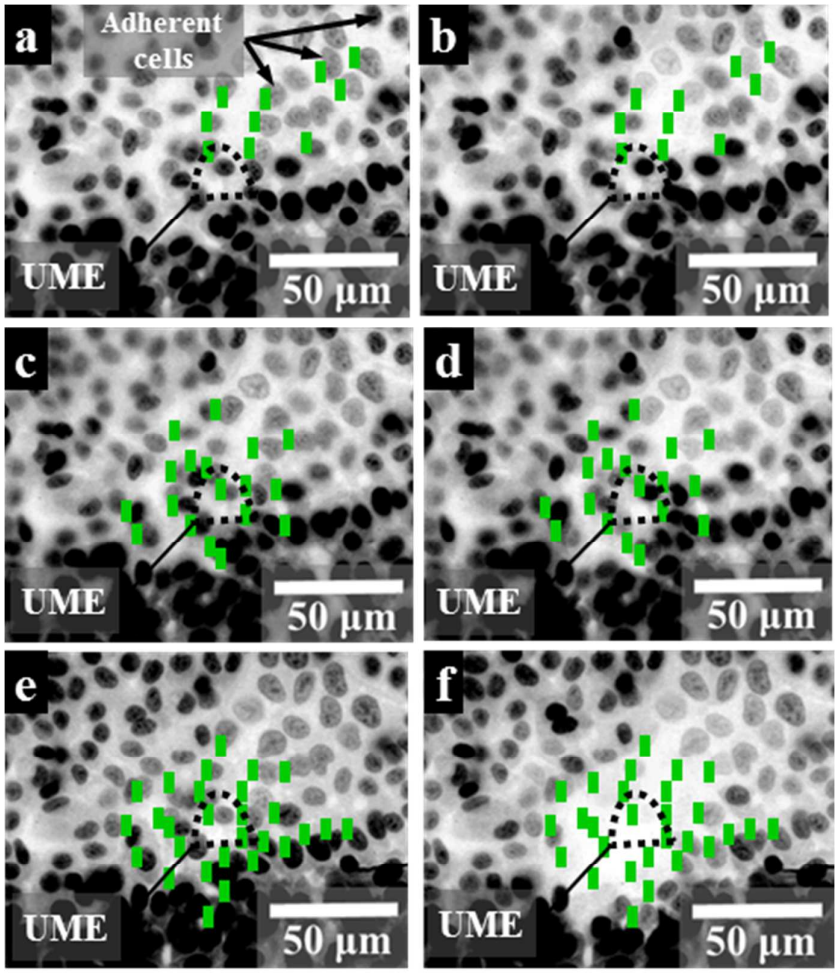

Figure S12. Fluorescence microscopy images of adherent cancer cells labeled with AO before ((a), (c) and (e)) and after ((b), (d) and (f)) their perturbation by using the electrochemical push-pull probe in an electrochemical mode. For a better visualization, all obtained images were converted into black-and-white, the colors were inverted and the brightness adjusted. The working distance *d* was 20 µm for a) and b), 15 µm for c) and d) and 10 µm for e) and f), the inclination angle was equal to 90°. Working electrode = integrated carbon paste UME, QRE = Ag, CE = Pt, applied potential = –2 V during a period of 180 s. Cells marked with green were significantly affected during the experiment.

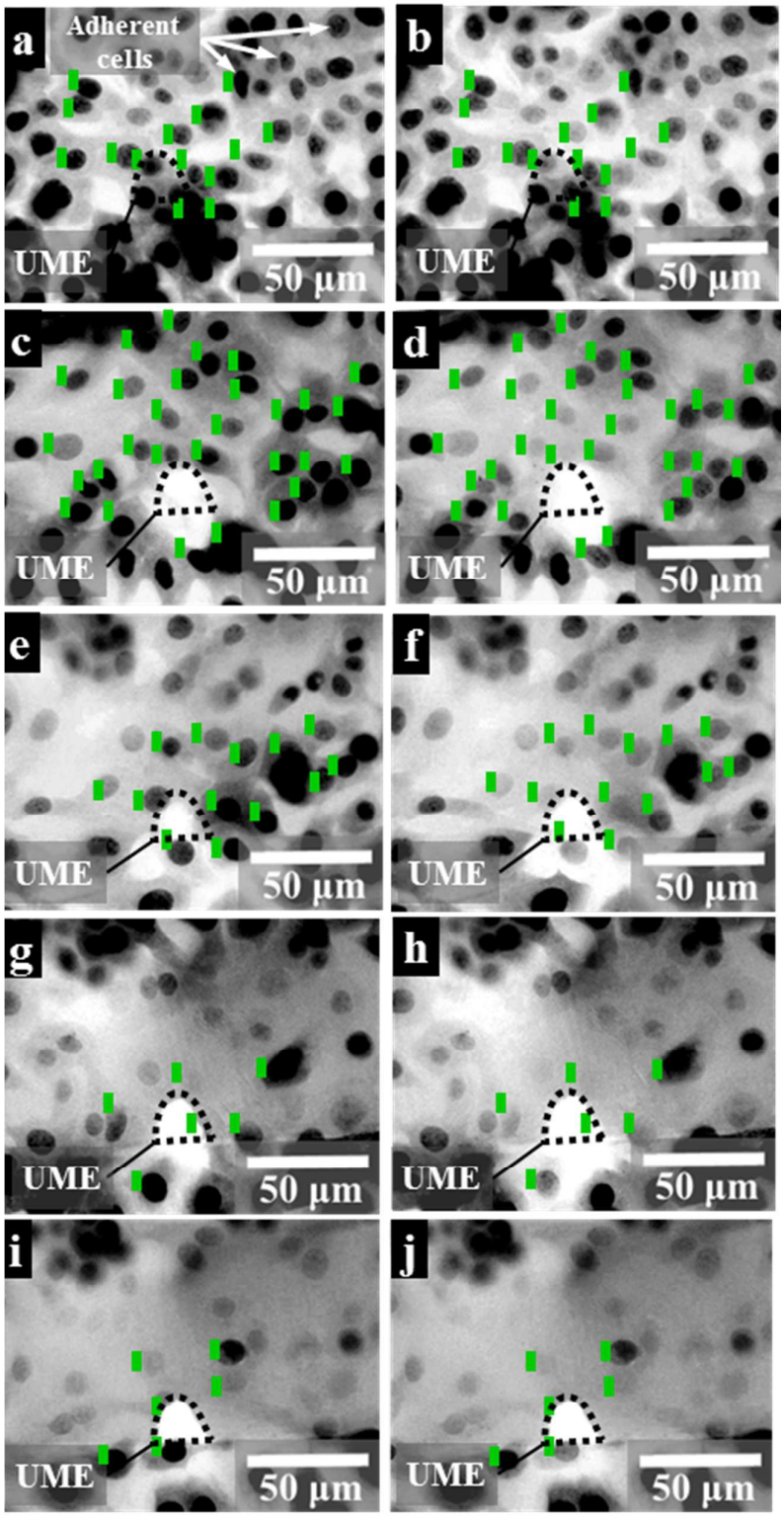

Figure S13. Fluorescence microscopy images of adherent cancer cells labeled with AO before ((a), (c) and (e)) and after ((b), (d) and (f)) their perturbation by using the electrochemical push-pull probe in an electrochemical mode. For a better visualization, all obtained images were converted into black-and-white, the colors were inverted and the brightness adjusted. The working distance *d* was 20 µm for a) and b), 15 µm for c) and d), 10 µm for e) and f), 5 µm for g) and h) and 2 µm for i) and, j). The inclination angle was equal to 70°. Working electrode = integrated carbon paste UME, QRE = Ag, CE = Pt, applied potential = –2 V during a period of 180 s. Cells marked with green were significantly affected during the experiment

Some adherent cells showed an increased intensity of the fluorescence after the electrochemical pH stimulation (Figures 5, S12 and S13). This phenomenon could be caused by two effects. On the one hand, the fluorescence spectrum of acridine orange presents a red shift when the pH of the media is increased, which means that during the pH gradient formation in the system, there are cells exposed to a pH at which the intensity of the fluorescence of acridine orange pass by a maximum in the excitation spectra at the detection wavelength. This hypothesis is also confirmed by the fact that the cells with the increased fluorescence intensity are mainly located at the edge of the affected area. On the other hand, the acridine orange uptake by cells is also dependent on pH with a nearly doubling[3] of the concentration when the pH shifts from 6.2 to 8.5.

References

(1) Albery, W. J.; Brett, C. M. A. *J. Electroanal. Chem.* **1983**, *148*, 201–210.

(2) Compton, R. G.; Greaves, C. R.; Waller, A. M. *J. Appl. Electrochem.* **1990**, *20*, 586–589.

(3) Elliot R., Philip I. M. *J. Cell Biol.* **1963**, *18*, 237–250).